THE JOURNAL OF BIOLOGICAL CHEMISTRY VOL. 285, NO. 17, pp. 12787–12802, April 23, 2010

Down-regulation of Protein-tyrosine Phosphatases Activates an Immune Receptor in the Absence of Its Translocation into Lipid Rafts*[S]

Received for publication, August 5, 2009, and in revised form, February 11, 2010 Published, JBC Papers in Press, February 15, 2010, DOI 10.1074/jbc.M109.052555

Petr Heneberg[‡1,2], **Lubica Dráberová**[‡1], **Monika Bambousková**[‡], **Petr Pompach**[§], **and Petr Dráber**[‡3]

From the [‡]*Laboratory of Signal Transduction, Institute of Molecular Genetics, and* [§]*Institute of Microbiology, Academy of Sciences of the Czech Republic, CZ-142 20 Prague 4, Czech Republic*

The earliest known biochemical step that occurs after ligand binding to the multichain immune recognition receptor is tyrosine phosphorylation of the receptor subunits. In mast cells and basophils activated by multivalent antigen-IgE complexes, this step is mediated by Src family kinase Lyn, which phosphorylates the high affinity IgE receptor (FcεRI). However, the exact molecular mechanism of this phosphorylation step is incompletely understood. In this study, we tested the hypothesis that changes in activity and/or topography of protein-tyrosine phosphatases (PTPs) could play a major role in the FcεRI triggering. We found that exposure of rat basophilic leukemia cells or mouse bone marrow-derived mast cells to PTP inhibitors, H_2O_2 or pervanadate, induced phosphorylation of the FcεRI subunits, similarly as FcεRI triggering. Interestingly, and in sharp contrast to antigen-induced activation, neither H_2O_2 nor pervanadate induced any changes in the association of FcεRI with detergent-resistant membranes and in the topography of FcεRI detectable by electron microscopy on isolated plasma membrane sheets. In cells stimulated with pervanadate, H_2O_2 or antigen, enhanced oxidation of active site cysteine of several PTPs was detected. Unexpectedly, most of oxidized phosphatases bound to the plasma membrane were associated with the actin cytoskeleton. Several PTPs (SHP-1, SHP-2, hematopoietic PTP, and PTP-MEG2) showed changes in their enzymatic activity and/or oxidation state during activation. Based on these and other data, we propose that down-regulation of enzymatic activity of PTPs and/or changes in their accessibility to the substrates play a key role in initial tyrosine phosphorylation of the FcεRI and other multichain immune receptors.

Multichain immune recognition receptors (MIRRs),[4] such as T- and B-cell receptors, NK receptors, and Fc receptors are transmembrane multiprotein complexes that are activated by binding of their ligands. The first detectable biochemical step after ligand binding is phosphorylation of tyrosine residues in the cytoplasmic domain of the receptor by protein-tyrosine kinases (PTKs) of the Src family. Signal propagation and termination are spatiotemporally regulated by proper interplay between a wide range of PTKs and protein-tyrosine phosphatases (PTPs). Even though the role of PTKs in the MIRRs signaling has been intensively studied (1, 2), the exact involvement of PTPs remains still enigmatic and only partially understood (3–5).

Most members of the PTP family are characterized by a signature motif (I/V)HC*XX*G*XX*R(S/T) in their catalytic domain. An invariant Cys residue present in this motif is essential for catalysis. Because this Cys has low pK_a value, it is present as a thiolate anion at neutral pH, which strengthens its ability to act in nucleophilic attack on the phosphate group in potential substrates. However, the low pK_a value also renders this residue highly susceptible to oxidation, which is followed by sharp inhibition of PTP activity (6), a part of which was found to be reversible *in vivo* (7).

Application of oxidative agents was shown to induce cellular activation independent of receptor triggering. In mast cells, exposure to pervanadate (a mixture of vanadate and H_2O_2 (8, 9)) was found to stimulate tyrosine phosphorylation of various proteins, followed by enhanced calcium uptake and degranulation (10, 11). Pervanadate causes oxidation and subsequent inactivation of PTPs (12). However, it is not known whether the key mast cell immunoreceptor, the high affinity IgE receptor (FcεRI), is tyrosine-phosphorylated in pervanadate-treated cells similarly to antigen-activated cells and, if so, whether this phosphorylation is due to a transfer of FcεRI into lipid rafts, as predicted by the lipid raft model (see below). Furthermore, it is

* This work was supported in part by Projects 301/09/1826 and P302/10/1759 from Grant Agency of the Czech Republic, Center of Molecular and Cellular Immunology 1M0506, Projects LC-545 and 1M0505 from the Ministry of Education, Youth, and Sports of the Czech Republic, Grants KAN200520701 and M200520901 from the Academy of Sciences of the Czech Republic, and Institutional Project AVOZ50520514.

[S] The on-line version of this article (available at http://www.jbc.org) contains supplemental Figs. S1 and S2 and Tables S1 and S2.

[1] Both authors contributed equally to this work.

[2] Supported by Research Goal MSM0021620814 from the 3rd Faculty of Medicine, Charles University, Prague, Czech Republic, and by a Canadian Institute of Health Research fellowship.

[3] To whom correspondence should be addressed: Laboratory of Signal Transduction, Institute of Molecular Genetics, Academy of Sciences of the Czech Republic, Videnska 1083, CZ-142 20 Prague 4, Czech Republic. Tel.: 420-241062468; Fax: 420-241062214; E-mail: draberpe@img.cas.cz.

[4] The abbreviations used are: MIRR, multichain immune recognition receptor; PTK, protein-tyrosine kinase; PTP, protein-tyrosine phosphatase; FcεRI, high affinity IgE receptor; ITAM, immunoreceptor tyrosine-based activation motif; DRM, detergent-resistant membrane; ROS, reactive oxide species; RBL, rat basophilic leukemia; FCS, fetal calf serum; BMMC, bone marrow mast cell; IL-3, interleukin-3; SCF, stem cell factor; TNP, trinitrophenyl; BSA, bovine serum albumin; mAb, monoclonal antibody; DNP, dinitrophenyl; SHP, Src homology 2 domain-containing phosphatase; HRP, horseradish peroxidase; GαMIgG, goat anti-mouse IgG; GαRIgG, goat anti-rabbit IgG; PCF, pair correlation function; IAA, iodoacetic acid; FDP, 3,6-fluorescein diphosphate; oxPTP, oxidized PTP; Pv, pervanadate; MALDI, matrix-assisted laser desorption ionization; HePTP, hematopoietic PTP.

not known whether or not FcεRI triggering leads to decreased activity of PTPs, an effect that would partly explain the enhanced tyrosine phosphorylation of FcεRI.

In mast cells and basophils activated by binding of multivalent antigen to IgE anchored to the FcεRI, initial tyrosine phosphorylation of the FcεRI β and γ subunits is catalyzed by the Src family kinase Lyn (13). The mechanism by which Lyn initiates phosphorylation of the FcεRI subunits has been extensively studied; two major models are being considered.

The transphosphorylation model is based on observation that a small fraction of Lyn is constitutively bound to FcεRI in the absence of immunoreceptor tyrosine-based activation motif (ITAM) phosphorylation. When FcεRI becomes aggregated, Lyn bound to one receptor can phosphorylate ITAMs on the adjacent receptor and thus initiate the signaling pathway (14). This model was recently supported by studies using trivalent ligands connected to DNA spacers of varying lengths, showing that phosphorylation of the receptor subunits and subsequent activation events require appropriate spatial organization of the FcεRI clusters (15). Furthermore, transfection of cDNA coding for the Lyn N-terminal domain, responsible for association of Lyn with nonaggregated FcεRI, has been shown to inhibit FcεRI β and γ subunits phosphorylation; this inhibition probably reflects a competition between endogenous Lyn kinase constitutively associated with FcεRI β and exogenous Lyn unique domain (16). Finally, electron microscopy studies of immunolabeled plasma membrane sheets demonstrated a colocalization of Lyn kinase with ~25% of FcεRI clusters in unstimulated cells (17).

The alternative model postulates that Lyn kinase is not preassociated with FcεRI but instead is separated from it into membrane microdomains called lipid rafts; this prevents Lyn-mediated FcεRI phosphorylation in nonactivated cells (18, 19). After activation, the aggregated (but not monomeric) FcεRI associates with membrane rafts, and only this pool of the FcεRI is tyrosine-phosphorylated after cross-linking. This model is supported by the experiments of Baird and co-workers (18, 19), who showed that Lyn kinase and FcεRI are located, respectively, in low and high density fractions of sucrose gradient after ultracentrifugation of lysates from nonactivated cells solubilized with Triton X-100. However, when FcεRI-activated cells were used and analyzed under the same conditions, the majority of both Lyn and FcεRI was found in low density fractions (18, 19). Although other plasma membrane receptors exhibit similar density-related changes after ligand-mediated triggering (20), most interpretations of these experiments presume that detergent-resistant membranes (DRMs) are equal to lipid rafts, an assumption that is probably incorrect (21, 22). Furthermore, electron microscopy studies indicated that FcεRI triggering did not lead to enhanced association of FcεRI aggregates with Lyn and some other presumable lipid raft markers (17). It should be mentioned in this connection that dimerization of FcεRI results in increased association of the receptor with DRMs without enhanced formation of large FcεRI aggregates (23). Furthermore, we found that genetic removal of the Lyn kinase palmitoylation site resulting in a release of Lyn from DRMs (but not plasma membrane) failed to inhibit Lyn-mediated FcεRI phosphorylation (24). Thus, the molecular mechanisms of initial stages of FcεRI signaling still remain unclear.

This study is focused on the role of PTPs in the regulation of cell signaling following external addition of reactive oxide species (ROS) or after FcεRI triggering. We investigated the oxidation state and enzymatic activity of various PTPs after exposure of mast cells to ROS at various concentrations, including those observed under physiological conditions in a close vicinity to activated macrophages, where cell-released ROS serve as mast cell proinflammatory agents (25). Because several PTPs are known to be involved in FcεRI signaling (3, 26–29), we also examined the influence of ROS on tyrosine phosphorylation of FcεRI and fine topography of FcεRI and oxidized PTPs. The findings indicate that ROS-induced inhibition of PTPs could lead to tyrosine phosphorylation of FcεRI in the absence of FcεRI movement into DRMs. This led us to postulate a third model of FcεRI signaling, which also takes PTPs into account.

EXPERIMENTAL PROCEDURES

Cells—Rat basophilic leukemia (RBL) cells, clone 2H3 (30), were kindly provided by H. Metzger. They were maintained as monolayers in culture medium consisting of a 1:1 mixture of RPMI 1640 and minimum essential medium supplemented with nonessential amino acids, 3 mM L-glutamine and 1 mM sodium pyruvate. This medium was further supplemented with antibiotics (penicillin (100 units/ml) and streptomycin (100 μg/ml)), extra D-glucose (2.5 mg/ml), and 10% (v/v) heat-inactivated fetal calf serum (FCS). The cultures were maintained at 37 °C in humidified atmosphere of 5% CO_2 in air. Cells grown as monolayers were dissociated with 0.2% EDTA in phosphate-buffered saline (PBS), pH 7.4, and subcultured 2 times a week.

Bone marrow mast cells (BMMCs) were isolated from the femurs and tibias of 6–10-week-old C57BL/6J mice. The cells were incubated for 6–8 weeks in suspension cultures in freshly prepared culture media (Iscove's medium containing 10% FCS and antibiotics) supplemented with interleukin-3 (IL-3; 20 ng/ml; PeproTech EC, London, UK) and stem cell factor (SCF; 40 ng/ml; PeproTech EC). Before activation, BMMCs were cultured for 16 h in culture medium without SCF, followed by incubation for 3–4 h in SCF- and IL-3-free medium supplemented with trinitrophenyl (TNP)-specific IgE (1 μg/ml). The cells were then washed in buffered saline solution (BSS: 20 mM HEPES, pH 7.4, 135 mM NaCl, 5 mM KCl, 1.8 mM $CaCl_2$, 5.6 mM glucose, 1 mM $MgCl_2$) supplemented with 0.1% bovine serum albumin (BSA) and challenged with various concentrations of TNP-BSA conjugate. Alternatively, cells were cultured for 16 h in culture medium without SCF, followed by incubation for 3–4 h in SCF- and IL-3-free medium, and activated with various concentrations of H_2O_2 or pervanadate as indicated under "Results." Cell cultures were mycoplasma-free as confirmed by the Hoechst staining method (31).

Antibodies and Reagents—The following mouse monoclonal antibodies (mAbs) were used: TNP-specific IgE (IGEL b4 1) (32), dinitrophenyl (DNP)-specific IgE (33), anti-oxidized PTP active site (oxPTP; clone 335636, R&D Systems, Minneapolis, MN), anti-Lyn (34), and anti-FcεRI β subunit (JRK) (35). Rabbit polyclonal antibodies specific for Src homology 2 domain-containing phosphatase (SHP)-1 (C-19), SHP-2 (C-18), hematopoi-

etic PTP (HePTP) (H-80), and PTP-MEG2 (H-300), the corresponding blocking peptide for SHP-2 antibody (sc-280 P), and a negative control peptide (sc-287 P) were obtained from Santa Cruz Biotechnology (Santa Cruz, CA). Phospho-Tyr-specific mAb (PY20), conjugated to horseradish peroxidase (HRP), was purchased from BD Transduction Laboratories (Lexington, KY). IgE-specific antibody was prepared by immunization of rabbits with isolated IGEL b4 1, followed by immunoaffinity purification of the rabbit anti-mouse IgE on immobilized IgE. Goat anti-mouse IgG (GαMIgG) affinity-purified secondary antibody conjugated to 5-nm colloidal gold particles were obtained from Amersham Biosciences. Goat anti-rabbit IgG (GαRIgG) affinity-purified antibodies conjugated to 6- or 12-nm gold particles were obtained from Jackson ImmunoResearch (West Grove, PA). EM streptavidin conjugated with 5-nm colloidal gold particles was obtained from BBInternational (Cardiff, UK). [γ-^{32}P]ATP was purchased from ICN (Irvine, CA). Nickel electron microscopy grids (300 mesh), OsO_4, and Pioloform were obtained from Christine Gröpl Elektronenmikroskopie (Tulln, Austria). Poly(Glu_4Tyr)$_n$ and all other chemicals were from Sigma. Pervanadate was prepared by mixing sodium orthovanadate solution with H_2O_2 to get a concentration of 10 mM for both components. After 15 min at 20 °C, the pervanadate solution was diluted 1:50 directly into solutions used for cell activation.

A peptide VHCSAG surrounding the catalytic site cysteine shared by all known catalytically active classical PTP domains was used in competition experiments to verify the specificity of oxPTP mAb (36). This and other peptides (see below) were obtained from GenScript (Piscataway, NJ). The sulfhydryl group of the cysteine was oxidized to sulfonic acid (–SO_3H) as described previously (37) with minor modifications. Briefly, performic acid was freshly prepared by mixing 88% formic acid with 30% H_2O_2 at a ratio 9:1. The peptide (7 mg) was dissolved in 100 μl of ice-cold 88% formic acid and mixed with 1.5 ml of performic acid. After 1 h of incubation on ice, 15 ml of water was added, and the mixture was freeze-dried. The peptide was dissolved in 2 ml of PBS, aliquoted, and stored at −70 °C. Control VHASAG peptide was treated in the same way. Other controls involved peptides VHCSAG and VHASAG treated with formic acid but not oxidized with performic acid. All peptides were analyzed by electrospray ionization/Fourier transformation mass spectrometry. The peptides were dissolved in solvent composed of 50% methanol in water and 0.1% formic acid. Thirteen picomolar solution of each peptide was used for the analysis. Peptides were ionized by electrospray Dual II ion source (Bruker Daltonics, Billerica, MA). Mass spectra were acquired on APEX-Qe Fourier transformation mass spectrometry instrument equipped with a 9.4 tesla superconducting magnet (Bruker Daltonics). The cell was opened for 4 ms, and accumulation time was set at 0.8 s; on average, one experiment consisted of 12 spectra. The acquisition data set size was set to 512,000 points with the mass range starting at m/z 200 atomic mass units. The instrument was externally calibrated by using arginine clusters resulting in mass error above 1 ppm. After a clean selection of the desired precursor, peptides have been confirmed by dropping the potential of the collision cell. Mass spectrometry confirmed complete oxidation of the peptide and the presence of three forms possessing 0–2 sodium ions (supplemental Fig. S1, *A* and *B*). The peptides were used for determining the specificity of oxPTP mAb. Immunoblotting studies showed that the binding of oxPTP mAb to the PTPs from pervanadate-oxidized cells was inhibited by the VHCSAG peptide only slightly yet strongly by the oxidized peptide, even though incompletely (supplemental Fig. S1*C*). VHASAG peptide treated with formic acid exhibited no change in molecular mass. Neither was the binding of oxPTP mAb to its targets inhibited. Importantly, oxPTP mAb bound only weakly to PTPs from nonactivated cells (see "Results").

Electron Microscopy of Immunogold-labeled Membrane Sheets—Ultraclean glass coverslips (15 mm in diameter) used for isolation of plasma membrane sheets were prepared as described previously (38). Coverslips used for attachment of BMMCs were coated in 24-well plates by overnight incubation at 4 °C with fibronectin (50 μg/ml in 0.43 M $NaHCO_3$), followed by washing with distilled water, and used immediately.

BMMCs (4×10^6/ml) were cultured in Iscove's medium with FCS, IL-3, and DNP-specific IgE (1 μg/ml). After 16–18 h, the cells were centrifuged and resuspended at a concentration of 10^7/ml in 1:4 mixture of PBS and Iscove's medium with FCS but without SCF, IL-3, and IgE. The suspension (0.2 ml) was transferred on fibronectin-coated coverslips in 24-well plates and incubated for 1 h at 37 °C. RBL cells were harvested by exposure to EDTA in PBS, counted, resuspended to 5×10^5 cells in 0.5 ml of complete culture medium supplemented with anti-DNP IgE (1 μg/ml), and transferred into wells of 24-well plate containing ultraclean glass coverslips.

The cells were washed with PBS, and FcεRI was aggregated by incubation with DNP-BSA (1 μg/ml) in a 4:1 mixture of PBS and culture medium for 5 min at 37 °C. Alternatively, the cells were activated by addition of 0.2 mM pervanadate at 37 °C. Cell activation was stopped by rapid washing out of the activators and immersing the coverslips with attached cells in ice-cold HEPES buffer (25 mM HEPES, pH 7.0, 25 mM KCl, 2.5 mM magnesium acetate). For surface labeling of FcεRI, IgE-sensitized cells were washed three times with ice-cold PBS and exposed on ice to rabbit anti-mouse IgE (1:200 diluted in PBS + 0.1% BSA, 10 min), followed by GαRIgG conjugated with 12 nm gold (10-fold diluted). Plasma membrane sheets were isolated immediately after activation, fixed by ice-cold 2% paraformaldehyde in HEPES buffer (10 min), and transferred into PBS where they were floated for 5–30 min. Labeling of the intracellular leaflet component was performed by incubation of the grids with membranes on drops of antibodies diluted in PBS + 0.1% BSA (30 min), followed by four 5-min washes with PBS. FcεRI β subunit and oxidized PTPs were labeled by sequential incubation of the membranes with primary mAb JRK (2 μg/ml) and oxPTP (5 μg/ml), respectively, followed by GαMIgG conjugated with 5 nm gold (20-fold diluted). In some experiments, anti-oxPTP mAb was diluted in PBS/BSA containing 2.5× diluted VHCSAG or ox-VHCSAG and incubated for 20 min at 25 °C before use.

SHP-2 was detected with anti-SHP-2 antibody, followed by GαRIgG conjugated to 6- or 12-nm gold particles. Specificity of anti-SHP-2 antibody was verified by inhibition of the binding

with SHP-2 blocking peptide (sc-280 P) but not negative control peptide (sc-287 P). The specimens were post-fixed with 2.5% glutaraldehyde in PBS for 10 min and washed with PBS for 30 min. They were then stained for 10 min with 1% OsO_4 in cacodylate buffer, washed three times for 5 min in water, incubated for 10 min with 1% aqueous tannic acid, washed three times for 5 min in water, and stained for 10 min with 1% aqueous uranyl acetate. Finally, samples were washed twice with water for 5 min, air-dried, and observed with FEI Morgagni 268 electron microscope (FEI Czech Republic, Brno, Czech Republic) operating at 80 kV. Typically, 10–20 micrographs covering 22.2–44.4 μm^2 of the cell surface were obtained from each grid; three independent experiments were made for each condition tested.

The coordinates of gold particles were determined by means of ImageJ (National Institutes of Health). Statistical evaluation of particles clustering of the same type was based on program Gold (39) using pair correlation function (PCF), which expresses the ratio of the density of gold particles at a given distance from a typical particle to the average density of such particles.

Immunoprecipitation and Immunoblotting—Cells were harvested, resuspended in culture medium to a concentration 1×10^6 cells/ml, and sensitized or not with IgE (IGEL b4 1; ascites diluted 1:1000). After 60 min at 37 °C the cells were washed in BSS/BSA and challenged with antigen (TNP/BSA) for the indicated time intervals. Alternatively, unsensitized cells were activated by externally added H_2O_2 at the indicated concentrations and time interval or by addition of 0.2 mM pervanadate. Toward the end of the activation period, the cells were briefly centrifuged, and the cell pellets were lysed in ice-cold lysis buffer (25 mM Tris-HCl, pH 7.5, 140 mM NaCl, 2 mM EDTA, 1 mM Na_3VO_4, protease inhibitor mixture, and 0.2% Triton X-100). When indicated, 0.5% Brij 96, 1% Triton X-100 or a mixture of 1% *n*-dodecyl β-D-maltoside, 1% Nonidet P-40 was used instead of 0.2% Triton X-100.

To release free cytoplasmic molecules, the cells were permeabilized by incubation for 5 min on ice in PBS supplemented with 0.1% saponin, 5 mM $MgCl_2$ and 1 mM Na_3VO_4; cytoplasmic components released into the supernatant were removed, and the cell "ghosts" were then extracted for 15 min on ice in lysis buffer supplemented with 1% Triton X-100 (34, 40). Cell lysates were centrifuged at 16,000 × *g* for 1 min at 4 °C, and postnuclear supernatants were directly analyzed by SDS-PAGE and immunoblotting. Alternatively, the proteins of interest in postnuclear supernatants were immunoprecipitated for 2 h at 4 °C using antibodies bound to UltraLink-immobilized protein A or protein G (Pierce). The beads were then washed with lysis buffer, and the bound proteins were eluted by boiling in Laemmli SDS-PAGE sample buffer.

To detect sulfenic and sulfinic acid forms of active PTP sites, an alkylation step was inserted before elution of the immunoprecipitated proteins as described previously (41). Briefly, 100 mM iodoacetic acid (IAA) in lysis buffer without detergents was added to the washed beads with immunoprecipitates for 30 min at room temperature in the dark. Following incubation with IAA, the immunoprecipitates were washed three times and incubated with 100 mM dithiothreitol. After 30 min, dithiothreitol was washed out, and the beads were incubated with pervanadate for 60 min. The beads were then washed, and the proteins were eluted and size-fractionated by SDS-PAGE. Immunoblotting was performed with selected concentrations of primary and HRP-labeled secondary antibodies or with HRP-labeled PY-20. Immunoblots were quantified by Luminescent Image Analyzer LAS-3000 (Fuji Photo Film Co., Tokyo, Japan).

Identification of Oxidized PTPs by Mass Spectrometry—BMMCs were activated by pervanadate (0.2 mM, 15 min) and then lysed in ice-cold lysis buffer supplemented with 5 mM iodoacetamide. The nuclei were removed by centrifugation, and postnuclear supernatant was supplemented with SDS (final concentration 0.5%). After heating at 95 °C for 5 min and centrifugation at 4 °C for 5 min at 14,000 × *g*, the supernatant was supplemented with 4 volumes of cold lysis buffer with 1% Nonidet P-40. Oxidized PTPs were immunoprecipitated by adding oxPTP mAb-armed protein G. Immunoprecipitated material was released from the beads by heating (95 °C, 5 min) in SDS-PAGE sample buffer. The proteins were then size-fractionated by SDS-PAGE. The spots of interest were cut from the gel, destained by a mixture of 100 mM ethylmorpholine acetate buffer and acetonitrile (1:1), and reduced by tris(2-carboxyethyl)phosphine hydrochloride. Reduced cysteines were then alkylated by 50 mM IAA. Gel pieces were washed three times with acetonitrile and water. Trypsin protease was added to the gel in digestion buffer (50 mM ethylmorpholine acetate buffer, 10% acetonitrile, pH 8.3). After overnight incubation, tryptic peptides were extracted from the gel by addition of 80% acetonitrile, 0.1% trifluoroacetic acid.

Extracted peptides were desalted by using Peptide Microtrap in the off-line holder (MichromBioresources, Auburn, CA). Each sample was spotted on one position of the 384 ground steel position MALDI plate (Bruker Daltonics, Billerica, MA). α-Cyano-4-hydroxycinnamic acid was used as a matrix (Bruker Daltonics). Samples were ionized by matrix-assisted laser desorption ionization (MALDI) using Dual II ion source (Bruker Daltonics). Mass spectra were acquired on a APEX-Qe Fourier transformation mass spectrometry instrument equipped with a 9.4 tesla superconducting magnet (Bruker Daltonics). The cell was opened for 4 ms; accumulation time was set at 0.2 s, and one experiment consists of the average of four spectra. The acquisition data set size was set to 512,000 points with the mass range starting at m/z 600 atomic mass units. The instrument was externally calibrated by using Bruker Daltonics calibration standard II resulting in mass error above 1 ppm. The spectra were processed by Data Analysis 4.0 software (Bruker Daltonics) and searched by Mascot search engine against the data base (SwissProt) created from all known *Mus musculus* proteins.

Density Gradient Fractionation—This method was performed as described before (24) with some modifications. Cells (2×10^7) were sensitized in suspension with ^{125}I-labeled TNP-specific IgE and activated or not as described in the legend to Fig. 1, *F* and *G*. The cells were lysed on ice in 0.8 ml of lysis buffer (10 mM Tris-HCl, pH 8.0, 50 mM NaCl, 10 mM EDTA, 1 mM Na_3VO_4, 10 mM glycerophosphate, protease inhibitor mixture for mammalian tissues (Sigma), 1 mM PMSF, and 0.06% Triton X-100). After 15 min, the lysate was homogenized by passing it

10 times through a 27-gauge needle and adjusted to 40% (w/v) sucrose by adding an equal amount of 80% sucrose. The gradient was formed by dispensing 0.2 ml of 80% sucrose to the bottom of the polyallomer tube 13 × 51 mm (Beckman Instruments, Palo Alto, CA), followed by 0.5 ml of 60% sucrose, 1.5 ml of 40% sucrose containing the cell lysate, and successive addition of 0.8 ml of 35% and 0.5-ml aliquots of 30, 25, 20, and 15% sucrose. The loaded tubes were centrifuged for 4 h at 200,000 × *g* using an SW 55 Ti rotor (Beckman Instruments). Twenty five 0.2-ml fractions were collected from the top of the gradient.

Association of oxidized PTPs with DRMs was determined by lysing the cells (2×10^7) in 0.8 ml of ice-cold lysis buffer as above containing 0.2% Triton X-100. Gradient was formed by adding 0.5 ml of 80% sucrose stock solution to the bottom of the tube, followed by 1.5 ml of 40% sucrose containing the cell lysate, 2 ml of 30% sucrose, and 1 ml of 5% sucrose. The tubes were centrifuged as above. Ten 0.5-ml fractions were collected. All but the most dense fraction were mixed with an equal amount of 2× SDS sample buffer without (RBL cells) or with (BMMCs) 2-mercaptoethanol and analyzed by SDS-PAGE.

In-tube and In-gel Phosphatase Assays—To detect the enzymatic activity of PTPs, we used in-tube SensoLyte phosphatase assay kit obtained from AnaSpec (San Jose, CA). Briefly, 3,6-fluorescein diphosphate (FDP) was used as a fluorogenic phosphatase substrate. Immunoprecipitates were incubated for 30 min in buffer containing FDP according to the manufacturer's instructions. The phosphatase activity was determined by means of Tecan Infinite M200 monochromator-based microplate reader (Tecan Austria, Grödig/Salzburg, Austria) with excitation at 485/9 nm and emission at 528/20 nm.

Changes in enzymatic activity of nonreceptor PTPs were detected by means of phosphatase in-gel assay (42). Compared with the in-tube assay, the in-gel PTP assay allows detection of PTP activity related to the molecules of specific molecular weight, which is helpful in analysis of both whole lysates and immunoprecipitates. However, it detects activity changes caused by covalent modifications (such as phosphorylation) only. Briefly, poly$(Glu_4Tyr)_n$ radiolabeled with [γ-^{32}P]ATP using recombinant human c-Src served as a substrate. It was incorporated in 10% SDS-polyacrylamide gel. Following electrophoresis, the SDS was removed from the gel, and the proteins in the gel were renatured by sequential treatment with 6 M guanidine hydrochloride, 0.04% Tween 20, and 0.3% 2-mercaptoethanol in renaturation buffers. PTP activity was determined in autoradiographs of dried gels as areas from which ^{32}P had been selectively removed. Fuji Bio-Imaging Analyzer Bas 5000 was used for quantification.

RESULTS

Tyrosine Phosphorylation of FcεRI in the Absence of Its Association with DRM—As shown previously, exposure of mast cells to pervanadate inhibited the enzymatic activity of PTPs and led to dramatically enhanced tyrosine phosphorylation of PTK substrates (10, 11, 43, 44). Importantly, most of the PTK substrates did not become phosphorylated if pervanadate was added to the cell lysates instead of intact cells (45). These data suggested that there exist preformed signaling assemblies containing PTKs, PTPs, and their substrates and that these complexes are destroyed after detergent solubilization of the cells (45, 46).

In the first series of experiments, we therefore addressed the question whether FcεRI β and γ subunits are tyrosine-phosphorylated in pervanadate-activated cells, similarly to antigen-activated cells, and whether this activation reflects an association of the FcεRI with DRMs. IgE-sensitized RBL cells were activated by exposure to antigen or pervanadate and solubilized in different detergents, and IgE-FcεRI complexes were immunoprecipitated from postnuclear supernatants. Data presented in Fig. 1, *A* and *B*, indicate that only weak tyrosine phosphorylation of the FcεRI β and γ subunits is detectable in nonactivated cells. After antigen-mediated triggering, β and γ subunits of the FcεRI exhibited enhanced phosphorylation. As expected, the extent of tyrosine phosphorylation depended on the detergent used. The strongest phosphorylation was observed in cells solubilized in 0.2% Triton X-100. Lower tyrosine phosphorylation of the FcεRI subunits was observed in cells lysed with 1% Triton X-100, 0.5% Brij 96, or a mixture of 1% lauryl maltoside and 1% Nonidet P-40. IgE immunoprecipitates also contained some coprecipitated proteins; the extent of their amount and/or phosphorylation was largely dependent on the detergent used for cell solubilization (Fig. 1*A*).

IgE immunocomplexes from pervanadate-activated cells likewise showed strong tyrosine phosphorylation of FcεRI β and γ subunits (Fig. 1*B*). Similarly to antigen-activated cells, the use of various detergents was decisive for the appearance of different tyrosine-phosphorylated proteins coprecipitating with IgE. Strong tyrosine phosphorylation of FcεRI β and γ subunits was also observed in cells activated by H_2O_2, but only at relatively high concentrations of the activator (≥5 mM; Fig. 1*C*). As H_2O_2 forms a gradient across the plasma membrane, the intracellular concentrations causing FcεRI β and γ phosphorylation are expected to be ~7 times lower (47). H_2O_2-induced phosphorylation of the FcεRI subunits was transient, as indicated by higher phosphorylation at 5 min compared with 15 min. Because RBL cells are neoplastic cells, we also subjected nontransformed mouse BMMCs to the same analysis. Data presented in Fig. 1, *D* and *E*, indicate that both cell types exhibited similar dynamics of FcεRI tyrosine phosphorylation after activation by antigen. In cells activated with pervanadate, the onset of phosphorylation was slower, but the extent of phosphorylation was higher compared with antigen-induced FcεRI phosphorylation.

The observed tyrosine phosphorylation of FcεRI subunits in H_2O_2- or pervanadate-treated cells could reflect the existence of preformed signaling assemblies containing PTKs, PTPs, and FcεRI as their substrate. Thus, inhibition of PTPs by H_2O_2 or pervanadate could change the equilibrium between PTKs and PTPs and phosphorylation of the receptor. Alternatively, both H_2O_2 and pervanadate could induce movement of FcεRI into lipid rafts where it could be phosphorylated by Lyn kinase, as proposed by the lipid raft hypothesis (see Introduction). Next, we analyzed properties of IgE-FcεRI complexes from antigen- or pervanadate-activated cells. The cells were solubilized with 0.06% Triton X-100 and fractionated by discontinuous sucrose density gradient centrifugation. The results confirmed previously published data that most of FcεRI from nonactivated RBL

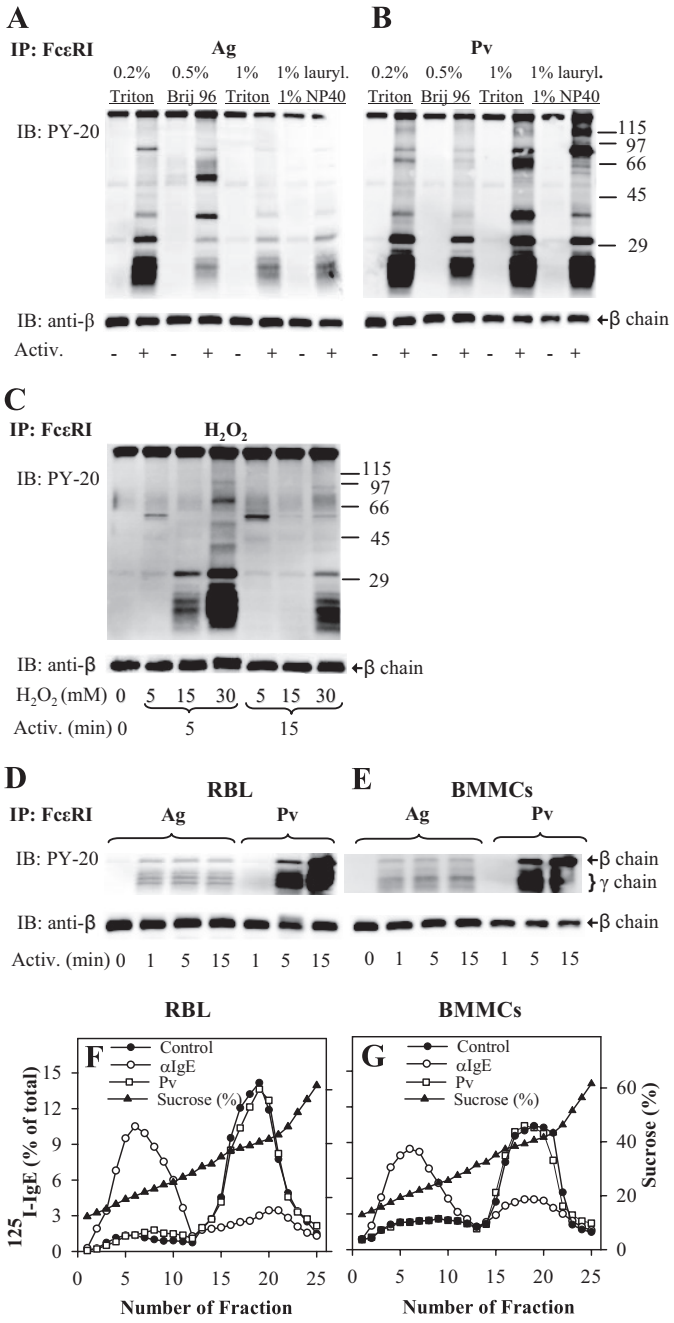

FIGURE 1. **Tyrosine phosphorylation of FcεRI in the absence of its association with DRMs.** *A*, IgE-sensitized RBL cells were activated (*Activ.*; +) or not (−) for 5 min with 0.5 μg/ml TNP-BSA (*Ag*). After activation, the cells were solubilized in lysis buffers containing 0.2% Triton X-100 (*Triton*), 0.5% Brij 96, 1% Triton X-100, or 1% *n*-dodecyl β-D-maltoside (*lauryl.*) and 1% Nonidet P-40 (*NP-40*). FcεRI receptor was immunoprecipitated (*IP*) from postnuclear supernatant using anti-IgE-armed protein A beads. The immunocomplexes were size-fractionated by SDS-PAGE and analyzed by immunoblotting (*IB*) with phosphotyrosine-specific antibody-HRP conjugates (*PY-20*). After stripping, the membranes were probed with antibody specific for FcεRI-β subunit (anti-β), which served as a loading control. *B*, IgE-sensitized RBL cells were activated (+) or not (−) for 5 min with 0.2 mM Pervanadate (Pv), solubilized, and analyzed as in *A*. *Numbers* on the *right* indicate positions of molecular mass markers (kDa). *C*, IgE-sensitized RBL cells were either not activated (0 min) or activated for 5 or 15 min with different concentrations (5–30 mM) of H_2O_2, then solubilized in lysis buffer containing 0.2% Triton X-100, and analyzed as in *A*. *D*, IgE-sensitized RBL cells were activated for different time intervals with 0.5 μg/ml TNP-BSA (*Ag*) or 0.2 mM Pv, then solubilized in lysis buffer containing 0.5% Triton X-100, and analyzed as in *A*. *E*, IgE-sensitized BMMCs were treated and analyzed as in *D*; only FcεRI β and γ subunits are shown (on the *right*). *F* and *G*, sucrose gradient ultracentrifugation of cell lysates. ^{125}I-IgE-sensitized RBL cells (*F*) and BMMCs (*G*) were exposed to anti-IgE (αIgE), 0.2 mM Pv, or BSS/BSA alone (*Control*). After 5 min, the cells were solubilized in lysis buffer containing 0.06% Triton X-100. Lysates were then diluted 1:1 with 80% sucrose buffer, loaded into sucrose step gradients, and ultracentrifuged. After fractionation, 0.2-ml aliquots were collected from the top of the gradient, and the distribution of ^{125}I-IgE-FcεRI complexes was expressed as percentage of total radioactivity present in individual fractions. Percentage of sucrose in the fractions was determined with Abbe refractometer. Representative data from two (*C*) or three (all other) experiments are shown.

cells is detergent-soluble and is found in high density fractions of sucrose gradient (fractions 15–25), whereas most of aggregated FcεRI localizes to low density fractions containing DRMs (fractions 1–12; Fig. 1*F*). In pervanadate-treated cells, most of FcεRI remained in the high density fractions, and no enhanced localization of the receptor in DRMs was observed. Similar results were obtained with BMMCs (Fig. 1*G*). Likewise, no movement of FcεRI into DRMs was observed in RBL cells or BMMCs activated for 5 min with 5 or 30 mM H_2O_2 (not shown). Thus, using two different cell types, we show that in pervanadate- or H_2O_2-activated cells FcεRI can be phosphorylated in the absence of its association with DRMs.

Topography of FcεRI—Previous studies showed that antigen-mediated activation of mast cells was accompanied by the formation of FcεRI aggregates in osmiophilic regions of the plasma membrane; it has been proposed that these aggregates could represent signaling assemblies required for initiation of FcεRI signaling (17, 48, 49). To find out whether or not there are any changes in topography of FcεRI observable after activation with pervanadate, RBL cells and BMMCs were activated by antigen-IgE complexes or pervanadate, and the distribution of the FcεRI β subunit was determined. Data presented in Fig. 2, *A* and *B*, confirm previous results that FcεRI in nonactivated cells is mostly distributed in small clusters in both RBL cells (17, 38) and BMMCs (38). In antigen-activated RBL cells or BMMCs, FcεRI accumulated in osmiophilic regions (Fig. 2, *C* and *D*). Contrary to that, when the cells were activated with pervanadate, FcεRI remained scattered in small clusters (Fig. 2, *E* and *F*) similar to those found in control nonactivated cells. These observations were confirmed by evaluation of particle clustering using PCF; in both RBL cells (Fig. 2*G*) and BMMCs (Fig. 2*H*), particle clustering was not affected by pervanadate treatment. Thus, phosphorylation of FcεRI can occur in the absence of association of FcεRI with DRMs and FcεRI clustering.

Enhanced Oxidation of PTPs in Activated Mast Cells—Pervanadate and H_2O_2 are known to inhibit the enzymatic activity of phosphatases by oxidation of their active site cysteine (50–52). Oxidation of reactive catalytic cysteine yields a reversibly oxidized sulfenic acid that is susceptible to further oxidation to sulfinic and sulfonic species. Oxidized forms of active site cysteine residue, especially the sulfinic and sulfonic species, can be detected with oxPTP antibody (53). In addition, reversibly oxidized forms of PTPs can be detected with oxPTP antibody after treatment of the lysates with IAA and pervanadate (41, 53).

To determine whether mast cell activation results in the formation of oxidized forms of phosphatases, we analyzed lysates of RBL cells by immunoblotting with oxPTP antibody. Interestingly, the antibody reacted with several phosphatases even in nonactivated cells (Fig. 3*A*, *Control*). Treatment of the cells

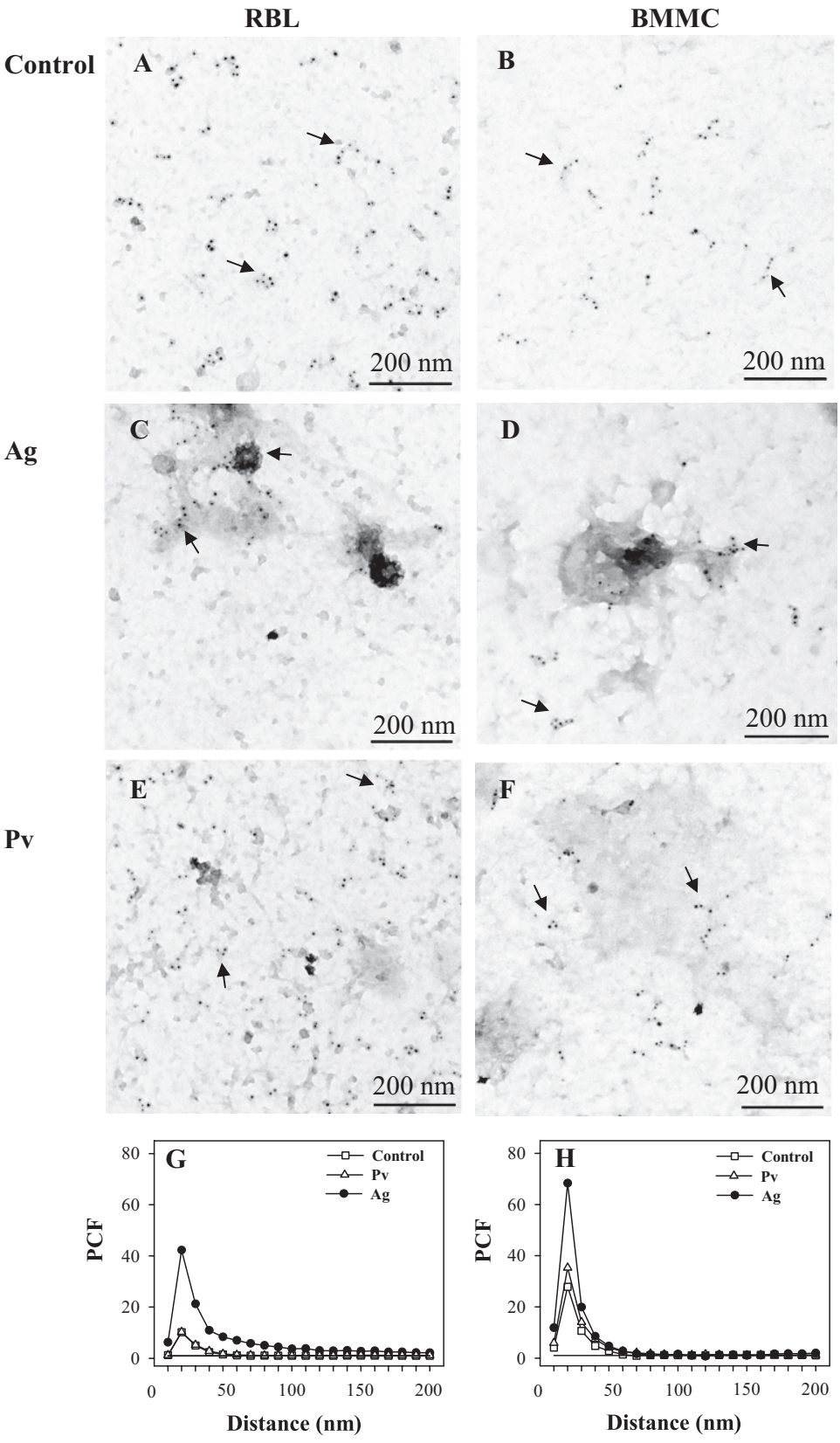

FIGURE 2. **Membrane topography of FcεRI-β subunit.** *A–F*, IgE-sensitized RBL cells (*A*, *C*, and *E*) or BMMCs (*B*, *D*, and *F*) were nonactivated (*Control*; *A* and *B*) or activated for 5 min with 1 μg/ml DNP/BSA (*Ag*; *C* and *D*) or 0.2 mM Pv (*E* and *F*). Membrane sheets were prepared and labeled from the cytoplasmic side for FcεRI-β subunit using JRK mAb followed by GαMIgG conjugated with 5-nm gold particles. *Arrows* indicate small clusters of FcεRI. *G* and *H*, clustering of FcεRI as determined by electron microscopy on membrane sheets (see above). PCF indicates clustering when it reaches the values higher than 1 arbitrary unit. Random distribution of gold particles (PCF = 1) is depicted by a *solid line*.

with H_2O_2 (5 mM, 15 min) enhanced the binding of oxPTP antibody to some of the PTPs, namely those with a relative molecular mass of 40–50 kDa. In pervanadate-activated cells (0.2 mM, 15 min), the antibody reacted more strongly with these PTPs and recently with PTPs of ~90 and 130–150 kDa. Antigen-mediated activation (0.5 μg/ml TNP/BSA, 15 min) enhanced the formation of oxidized forms to an extent similar to that induced by external addition of H_2O_2.

Partially different pattern of oxidized phosphatases was observed with BMMCs, and again the strongest binding of the antibody was seen in lysates from pervanadate-activated cells (Fig. 3*B*). Interestingly, each of the three stimuli led to comparably enhanced oxidation of PTP of about 95 kDa.

When RBL cells were exposed to 1.6 mM H_2O_2, the extent of oxidation of several PTPs rose in time following H_2O_2 addition (Fig. 3*C*). PTP oxidation also increased with a rising dose of H_2O_2 (Fig. 3*D*). Lysis of the cells before exposure to H_2O_2 also led to the formation of oxidized forms of PTPs, but the extent of this oxidation was lower than in intact cells (compare Fig. 3, *D* and *E*), suggesting that the proper regulation of enzymatic activity of phosphatases by ROS requires intact cellular environment. If BMMCs were exposed to various concentrations of H_2O_2, a dose-dependent increase in PTPs oxidation was also observed (Fig. 3*F*). It should be noted that H_2O_2 at all concentrations and time intervals analyzed was not toxic to the cells as determined by trypan blue exclusion test.

In an attempt to identify which PTPs were oxidized, we employed immunoprecipitation with oxPTP mAb, followed by size fractionation of the proteins by SDS-PAGE and mass spectrometry. Because oxPTP mAb does not precipitate native PTPs, the lysates were denatured by boiling with SDS and then "neutralized" with Nonidet P-40. Under these conditions, we were able to identify by mass spectrometry two

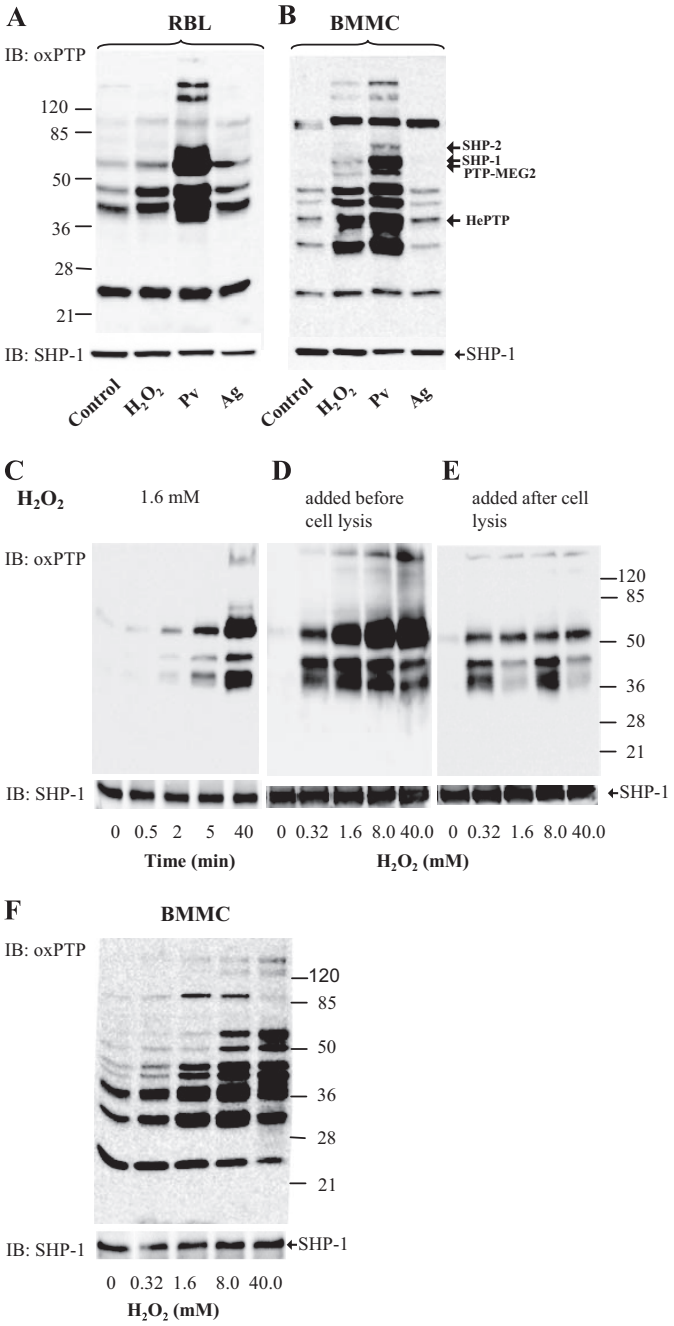

FIGURE 3. **Numerous PTPs are oxidized in the course of mast cell activation**. *A* and *B*, IgE-sensitized RBL cells (*A*) or BMMCs (*B*) were nonactivated (*Control*) or activated with 5 mM H_2O_2, 0.2 mM Pv, or TNP/BSA (*Ag*; 0.5 μg/ml). After 15 min, the cells were solubilized in lysis buffer containing 0.2% Triton X-100. Postnuclear supernatants were size-fractionated by SDS-PAGE and analyzed by immunoblotting (*IB*) with mAb specific for the oxidized PTP active site. After stripping, the membranes were probed with anti-SHP-1 antibody as a loading control (SHP-1). *Numbers* on the *left* and *right* indicate, respectively, position of molecular mass markers (in kDa) and localization of phosphatases as identified by immunoprecipitation and/or mass spectrometry (see supplemental Fig. S2 and Tables S1 and S2). *C*, RBL cells were activated with 1.6 mM H_2O_2 for the indicated time intervals. The cells were lysed and processed as in *A*. *D*, RBL cells were activated for 40 min with different concentrations of H_2O_2. Subsequently, the cells were lysed in 0.2% Triton X-100 and processed as in *A*. *E*, RBL cells were first lysed with 0.2% Triton X-100, and the postnuclear supernatants were exposed to H_2O_2 at the indicated concentrations. After 40 min, the lysates were fractionated by SDS-PAGE and analyzed as in *A*. *F*, BMMCs were activated for 40 min with different concentrations of H_2O_2. Subsequently, the cells were lysed in 0.2% Triton X-100 and processed as in *A*. Typical experiments from at least three performed are shown.

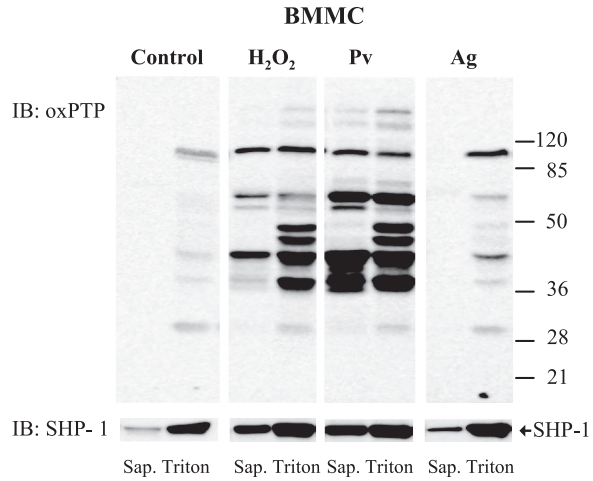

FIGURE 4. **Most of oxidized PTPs are associated with large molecular assemblies.** BMMCs were either nonactivated (*Control*) or activated with 5 mM H_2O_2, 0.2 mM Pv, or TNP/BSA (*Ag*; 0.5 μg/ml). After 5 min, the cells were permeabilized with 0.1% saponin, and the material released from the cells was removed (*Sap.*). The cell ghosts were then extracted for 15 min on ice in lysis buffer supplemented with 1% Triton X-100, and the postnuclear supernatant (*Triton*) was harvested. Both supernatants, saponin and Triton, were size-fractionated by SDS-PAGE and analyzed by immunoblotting (*IB*) with oxPTP mAb and after stripping with anti-SHP-1 antibody to check for the amount of this phosphatase (*bottom, arrow*). Representative data from three experiments are shown. *Numbers* on the *right* indicate positions of molecular mass markers (kDa).

oxidized PTPs as follows: SHP-1 (supplemental Table S1) and SHP-2 (supplemental Table S2). We also performed reverse experiments in which various PTPs were immunoprecipitated with the corresponding antibodies, and their oxidized forms were identified by immunoblotting with oxPTP mAb. By using this approach, we confirmed oxidation of the above-mentioned two PTPs and found two new ones, HePTP and PTP-MEG2 (supplemental Fig. S2). The position of the oxidized PTPs is indicated in Fig. 3*B*.

Subcellular Distribution of Oxidized Phosphatases—It is still unclear what are the phosphatases directly involved in the regulation of FcεRI phosphorylation. PTPs can be divided into cytosolic PTPs and receptor PTPs. To determine whether oxidized PTPs are freely moving in cytosol, or rather participate in the formation of large signaling assemblies, we employed a simple method based on the release of free cytoplasmic components from the cells permeabilized with the cholesterol-sequestering reagent saponin (42). Saponin-treated cells were first washed to remove free cytoplasmic components, then treated with Triton-X-100 to completely solubilize all membrane components, including DRMs, and subjected to immunoblotting analysis. By using this procedure, we found that almost all oxidized PTPs in nonactivated cells were localized to large molecular assemblies not released from the saponin-permeabilized cells but made soluble by the subsequent Triton X-100 solubilization step (Fig. 4, *Control*). In H_2O_2- or pervanadate-activated cells, a fraction of oxidized PTPs was found to be released from saponin-permeabilized cells. Some other PTPs, such as those of 40 and 45–50 kDa, were mostly associated with saponin-resistant cell ghosts, suggesting that they are part of large complexes. Antigen-induced activation led to enhanced oxidation of phosphatases of 45, 50, 70, and 90 kDa, all of which were

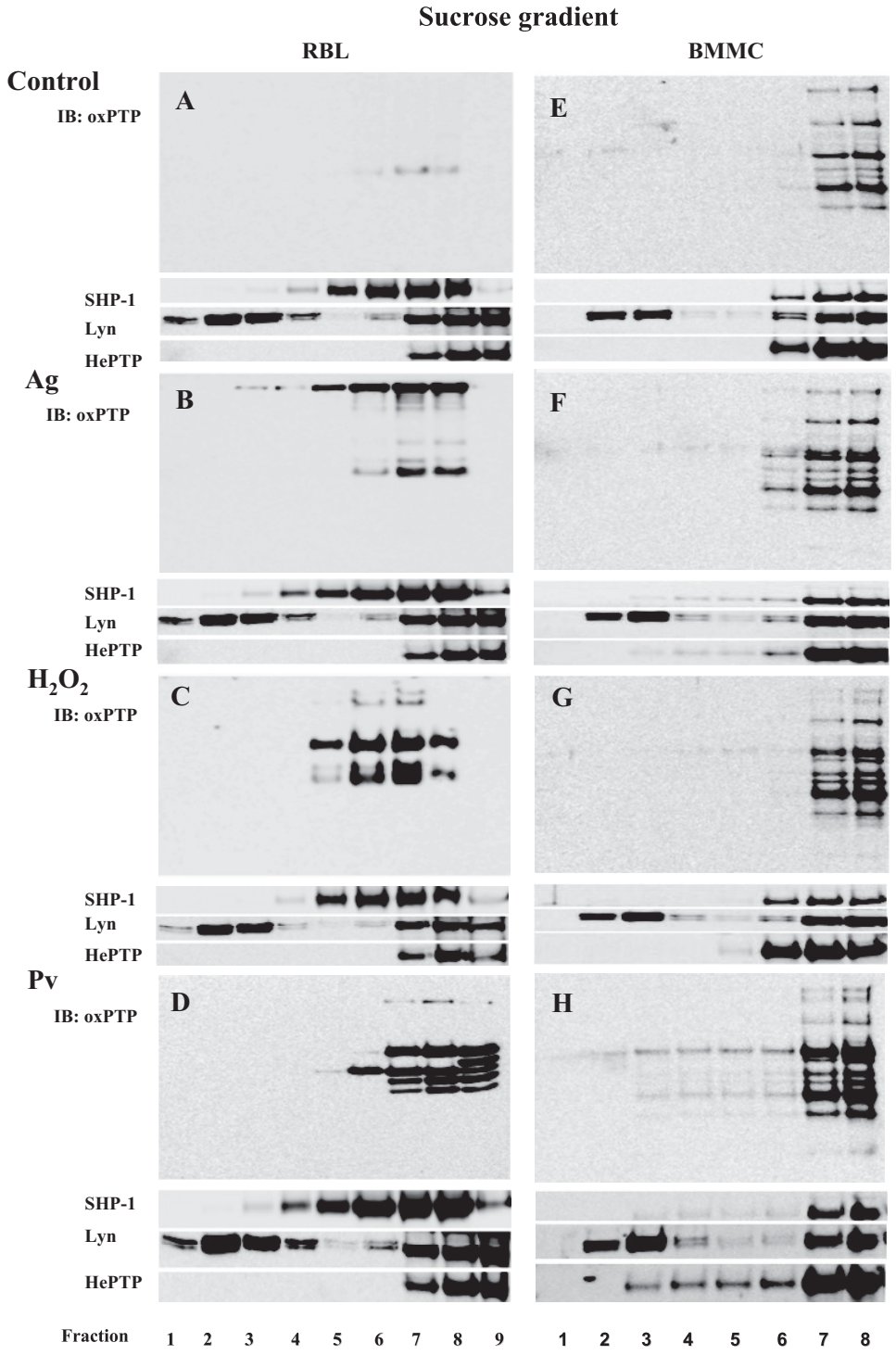

FIGURE 5. **Oxidized PTPs are excluded from DRMs.** *A*, nonactivated RBL cells (*Control*) were lysed in 0.2% Triton X-100 and then subjected to sucrose density gradient ultracentrifugation. Individual fractions were collected from the top and analyzed with oxPTP mAb by immunoblotting (*IB*) for the presence of oxidized PTP. *B*, IgE-sensitized RBL cells were activated for 5 min with TNP/BSA (*Ag*; 0.5 μg/ml) and then analyzed as in *A*. *C*, RBL cells were activated with 1.6 mM H_2O_2 for 40 min and then analyzed as in *A*. *D*, RBL cells were activated with 0.2 mM Pv for 5 min and then analyzed as in *A*. *E–H*, BMMCs were nonactivated (*E*) or activated by antigen (*F*), H_2O_2 (*G*), or pervanadate (*H*) as RBL cells (see above). Distribution in individual fractions of Lyn kinase (a marker of membrane rafts), SHP-1, and HePTP is also shown. Representative data from three experiments are shown.

associated with large signaling assemblies. The same samples were also used to determine the distribution of SHP-1. In nonactivated cells most of SHP-1 was associated with large signaling assemblies and was not released from saponin-permeabilized cells. After FcεRI triggering, and especially after treatment with H_2O_2 or pervanadate, more SHP-1 was released from permeabilized cells. It seems to indicate that SHP-1 was released from submembrane signaling complexes into the cytoplasm as a consequence of changes in affinity to a wide range of substrates, as in the case of the SHP-1 Cys/Ser mutant (54, 55).

Next, we studied the association of PTPs and their oxidized forms with DRMs. RBL cells and BMMCs were solubilized with 0.2% Triton X-100, followed by sucrose density gradient ultracentrifugation. Individual fractions were probed by immunoblotting with oxPTP mAb or antibodies specific for SHP-1, Lyn kinase, or HePTP. Data presented in Fig. 5, *A–H,* indicate that a significant fraction of Lyn kinase was localized as expected in DRMs (fractions 2–4), whereas SHP-1 and HePTP were found mostly in the high density fractions and only a minor part (0–5%, $n = 3$) in low density fractions. In nonactivated RBL cells, only a small fraction of PTPs was oxidized, and all were detected in the high density fractions (Fig. 5*A*). Antigen-mediated activation resulted in enhanced oxidation of several phosphatases, and again, all of them were in the high density fractions (Fig. 5*B*); the observed staining of the high molecular weight proteins, those located even in low density fractions, reflects the reactivity of the secondary HRP-labeled antibody with IgE bound to FcεRI. After treatment with H_2O_2 (Fig. 5*C*) or pervanadate (Fig. 5*D*), oxidized forms were again found only in the high density fractions. When BMMCs were analyzed, an enhanced amount of oxidized PTPs after activation with antigen, H_2O_2, or pervanadate was observed mainly in the high density fractions (Fig. 5, *E–H*). These data indicate that oxidized forms of PTPs are not associated with DRMs or that 0.2% Triton X-100 removes them from these regions, similarly as Syk is stripped off from FcεRI in antigen-activated cells (56).

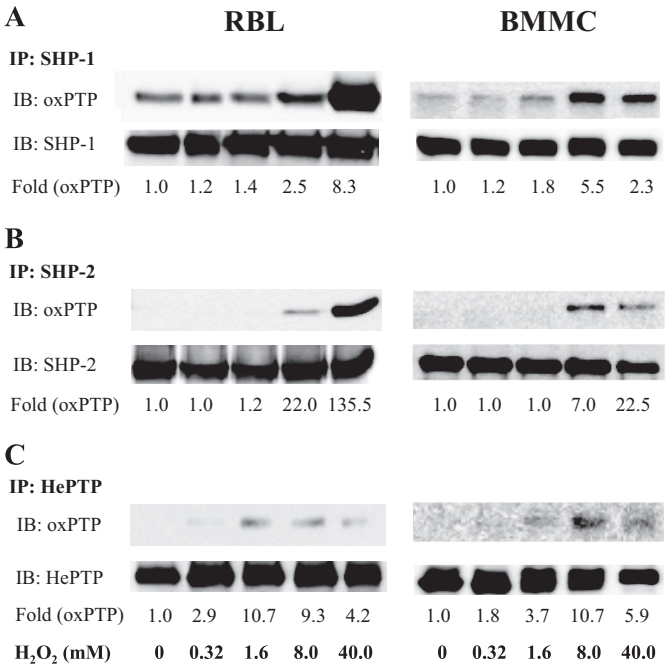

FIGURE 6. **Changes in oxidation of selected PTPs in H_2O_2-activated cells.** *A–C*, RBL cells (*left*) and BMMCs (*right*) were activated with the indicated concentrations of H_2O_2. After 40 min, the cells were lysed in 0.2% Triton X-100, and SHP-1 (*A*), SHP-2 (*B*) and HePTP (*C*) were immunoprecipitated (*IP*) from the postnuclear supernatants with the corresponding antibodies. After size fractionation by SDS-PAGE, the samples were subjected to immunoblotting (*IB*) with oxPTP mAb and subsequently, after stripping, with the respective antibodies as loading controls. The amounts of immunoprecipitated phosphatases and their oxidized forms were quantified by densitometry, and oxPTP signals were normalized to nonactivated cells and amount of the phosphatases (*Fold* (*oxPTP*)). Representative data from three experiments are shown.

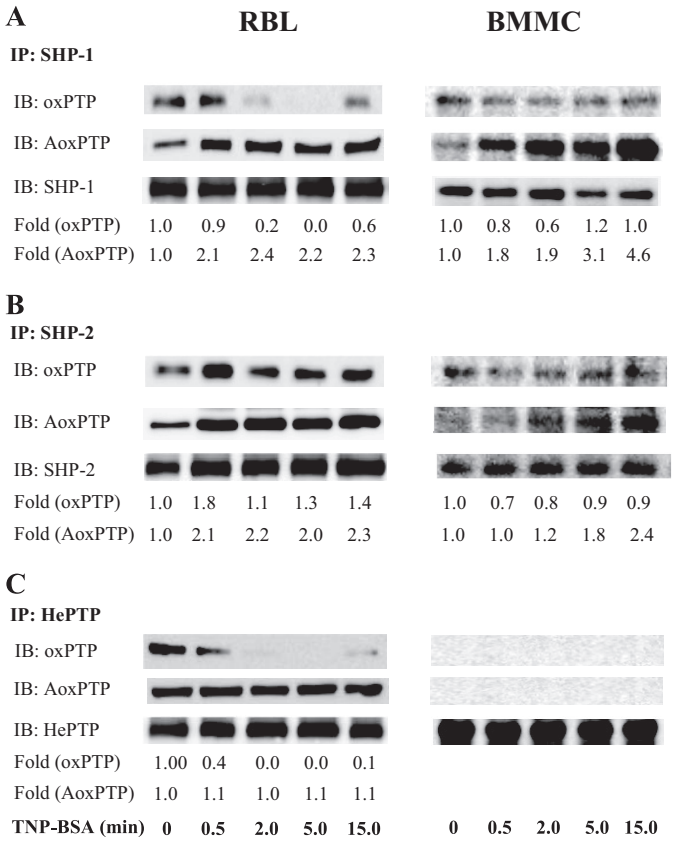

FIGURE 7. **Changes in oxidation of selected PTPs in cells activated by FcεRI triggering.** *A–C*, IgE-sensitized RBL cells (*left*) and BMMCs (*right*) were activated with 1 μg/ml TNP/BSA. After the indicated time intervals, the cells were lysed in 0.2% Triton X-100, and SHP-1 (*A*), SHP-2 (*B*), or HePTP (*C*) were immunoprecipitated (*IP*) from the postnuclear supernatants. After size fractionation by SDS-PAGE, the samples were analyzed by immunoblotting (*IB*) with oxPTP mAb (oxPTP, irreversibly oxidized). In parallel, another set of the immunoprecipitates was subjected to alkylation by IAA, followed by reduction of the reversibly oxidized PTPs with dithiothreitol, and by final oxidation with pervanadate (*IB*, AoxPTP, reversibly oxidized). After stripping the membranes were analyzed by immunoblotting with the corresponding antibodies (loading controls). The amounts of immunoprecipitated phosphatases and their oxidized forms were quantified by densitometry, and oxPTP and AoxPTP signals were normalized as in Fig. 6. Representative data from three experiments are shown.

Differences in Redox Regulation of Selected PTPs—The experiments just described showed that mast cells possess oxidized PTPs and that their amount increases in the course of cell activation. In further studies we investigated the redox regulation of phosphatases known to be involved in FcεRI signaling, namely SHP-1, SHP-2, and HePTP (26–29). In the first series of experiments, the phosphatases were immunoprecipitated from nonactivated or H_2O_2-treated RBL cells or BMMCs, and their oxidation was determined by immunoblotting with oxPTP antibody. Binding of PTP-specific antibodies served as loading controls. We found that a fraction of SHP-1 was oxidized even in nonactivated cells. After exposure to H_2O_2, especially at higher concentrations (8 and 40 mM), this oxidation was enhanced in both cell types (Fig. 6*A*). The closely related phosphatase SHP-2 showed no oxidation in quiescent cells and rising oxidation at higher concentrations of H_2O_2 (Fig. 6*B*). The maximum oxidation level of the active site Cys in SHP-2 was lower when compared with SHP-1. Finally, we also estimated the redox regulation of the active site of nonreceptor phosphatase HePTP, which reached a plateau of oxidation in RBL cells at 1.6 mM H_2O_2 and in BMMCs at 8.0 mM H_2O_2 (Fig. 6*C*). The maxima of HePTP oxidation were low, close to the detection limits. Thus, different PTPs in different cell types exhibit different basal levels of oxidation and sensitivity to redox regulation.

FcεRI Triggering Results in Changes of Redox State of Mast Cell PTPs—Similar experiments as above were performed with cells activated by antigen-induced aggregation of FcεRI. Because the oxPTP antibody reacts preferentially with the sulfonic acid form of the PTP active site, we also employed alkylation of the oxidized active sites to determine the sulfenic and sulfinic acid forms. Alkylation using IAA, followed by incubation in buffer containing dithiothreitol, and subsequently in buffer with pervanadate, resulted in a somewhat different pattern than in previous experiments. When SHP-1 was isolated from RBL cells activated for various time intervals with antigen, a substantial decrease of sulfonic acid form was observed, reaching the minimum at 5 min after triggering and returning back at 15 min (Fig. 7*A*, *IB: oxPTP*). This decrease could reflect the calpain-mediated degradation of oxidized forms of the PTPs (57). Unlike that, the levels of reversibly inactivated SHP-1 showed a rapid increase (within 30 s) after triggering with antigen, followed by constant levels between 0.5 and 15 min (Fig. 7*A*, *IB: AoxPTP*). The amount of irreversibly oxidized phosphatases in BMMCs only slightly decreased, whereas the amount of reversibly oxidized phosphatases steadily increased up to 15 min.

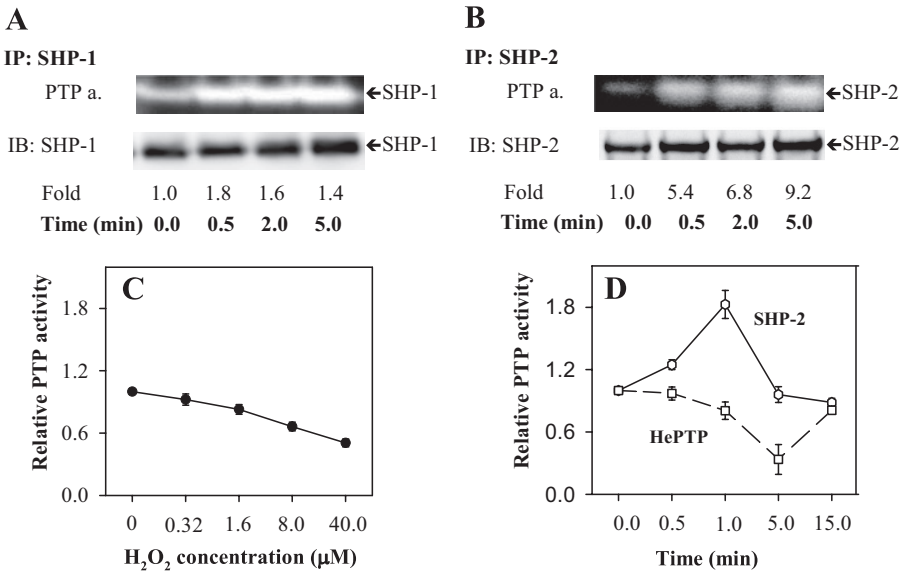

FIGURE 8. **Changes in activity of PTPs in activated cells.** *A* and *B*, IgE-sensitized RBL cells were activated with 1 μg/ml TNP/BSA for the indicated time intervals. After activation, the cells were permeabilized with saponin, and cell ghosts were subsequently lysed in lysis buffer supplemented with 1% Triton X-100. SHP-1 (*A*) and SHP-2 (*B*) were immunoprecipitated (*IP*) from the postnuclear supernatants, size-fractionated by SDS-PAGE, and subjected to the PTP in-gel assay (*PTP a.*). In parallel, the immunoprecipitated PTPs were also analyzed by immunoblotting (*IB*) with the corresponding antibodies as loading controls. The signals were evaluated by densitometry, and the enzymatic activity at each given time interval was normalized to nonactivated cells and amount of protein (*Fold*). Representative data from three independent experiments are shown. *C*, RBL cells were activated for 40 min with the indicated concentrations of externally added H_2O_2. Relative activity of total cellular PTPs was determined by fluorometry after addition of FDP to intact cells. *D*, IgE-sensitized RBL cells were activated with antigen (1 μg/ml TNP/BSA) for the indicated time intervals and lysed in 0.2% Triton X-100. Subsequently SHP-2 (*solid line*) and HePTP (*dashed line*) were immunoprecipitated, and relative activity of PTPs was determined by measuring FDP fluorescence. Averages ± S.D. from three to four experiments are shown.

Some irreversibly oxidized forms were observed in SHP-2 immunoprecipitates from nonactivated RBL cells and BMMCs. This is probably caused by a sensitization process because SHP-2 in nonsensitized and nonactivated cells did not react with oxPTP (Fig. 6*B*; H_2O_2 untreated cells). After activation with antigen, an increase in the number of sulfonic acid forms was observed 30 s after triggering in RBL cells; in BMMCs, a small decrease rather than increase of this form was observed (Fig. 7*B*, *IB: oxPTP*). The levels of reversibly oxidized SHP-2 increased within 30 s after activation and remained higher up to 15 min in both cell types (Fig. 7*B*, *AoxPTP*). When immunoprecipitated HePTP was analyzed, a reduction of its Cys-SO_3H form to almost undetectable levels was observed within 2 and 5 min after triggering in RBL cells. In BMMC, neither binding of IgE (sensitization) nor antigen triggering led to any detectable sulfonic acid (Fig. 7*C*, *IB: oxPTP*). HePTP from IgE-sensitized RBL cells carried some reversibly oxidized cysteine, and their levels remained constant in the course of activation, whereas this form was undetectable in BMMCs (Fig. 7*C*, *IB: AoxPTP*). These data indicate that FcεRI-induced activation of the cells initiates changes in the oxidation state of active site cysteine in SHP-1 and SHP-2 in both RBL cells and BMMCs. Some changes in redox state of HePTP were observed only in RBL cells in connection with cell sensitization.

Changes in Activity of Selected PTPs in Response to FcεRI Triggering—The observed changes of the redox state of PTPs in the course of cell activation suggested that their enzymatic activity is affected. To verify this hypothesis, we next assayed the enzymatic activity of several phosphatases by means of two assays, phosphatase in-gel assay using [γ-^{32}P]ATP and phosphatase in-tube assay employing fluorogenic phosphatase substrate FDP. When SHP-1 was immunoprecipitated from large signaling assemblies of saponin-permeabilized nonactivated cells (0 min), the basal level of phosphatase activity was determined. After FcεRI triggering, the enzymatic activity of SHP-1 slightly increased peaking at 30 s (Fig. 8*A*). Enzymatic activity of SHP-2 exhibited a more rapid increase (Fig. 8*B*).

The regulation of PTPs by oxidation, conformational changes, and/or phosphorylation may sometimes act against each other. We have confirmed the previous observations (12) that application of H_2O_2 to the cells leads to a substantial decrease in overall PTP activity detected at the level of FDP fluorescence (Fig. 8*C*). However, individual phosphatases may behave differently in the course of cellular activation induced by MIRRs, where the redox regulation is just one of several contributors. Using the in-tube FDP assay, we next compared the phosphatase activity of two selected nonreceptor PTPs, SHP-2 and HePTP isolated from total cell lysates, in the course of FcεRI activation. SHP-2 showed a substantial rapid transient increase of its activity (peaking at 1 min after triggering), whereas HePTP exhibited a clear decrease with the minimum at 5 min after activation (Fig. 8*D*). Thus, cell activation affects differentially the redox state, phosphorylation, and activity of PTPs.

Fine Topography of Oxidized PTPs—The finding that oxidized PTPs are part of the large signaling assemblies associated with saponin-permeabilized cells suggested that they are bound to the plasma membrane. This assumption was tested experimentally. When plasma membrane sheets were isolated from nonactivated cells and probed on the cytoplasmic side for oxidized PTPs, a limited number of particles (~2/μm^2) was observed (Fig. 9, *A* and *G*). An increased number of oxidized PTPs was detected in antigen-activated cells, thus supporting the previous results (Fig. 4) and extending them by localizing the phosphatases on the plasma membrane. Interestingly, oxidized forms of PTPs were mostly localized in distinct membrane cytoskeleton-like structures (Fig. 9, *B* and *G*). In cells activated by pervanadate, the number of membrane-associated particles was dramatically enhanced, and again, most of them were associated with the membrane cytoskeleton-like structures (Fig. 9, *C* and *G*). Although the ox-VHCSAG peptide was a suboptimal inhibitor of the binding of oxPTP mAb to oxidized phosphatases (see "Experimental Procedures"), this peptide, compared with nonoxidized control peptide, significantly

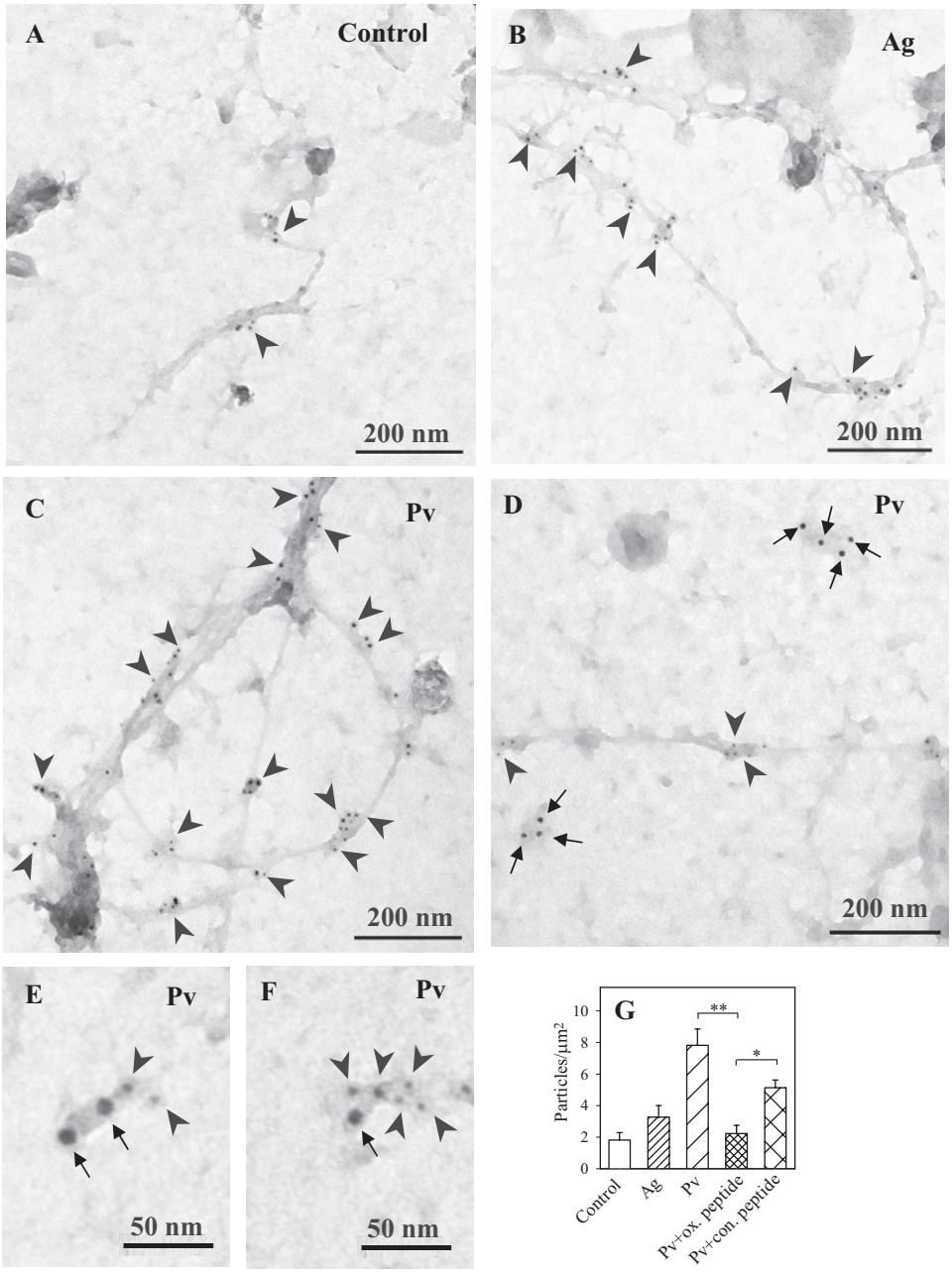

FIGURE 9. **Membrane topography of oxidized PTPs.** Plasma membrane sheets were isolated from nonactivated (control) IgE-sensitized (*A*), antigen (*Ag*)-activated (*B*; 1 μg/ml DNP-BSA, 5 min) or Pv-activated (*C*; 0.2 mM, 5 min) BMMCs. Membrane sheets were labeled from the cytoplasmic side with oxPTP mAb followed by GαMIgG conjugated with 5-nm gold particles (*arrowheads*). *D–F*, IgE bound to FcεRI was visualized by labeling whole cells (kept on ice) with rabbit anti-mouse IgE (*RαMIgE*), followed by GαRIgG conjugated with 12-nm gold (*arrows*); plasma membrane sheets were then isolated, and oxidized PTPs were detected as above. *G*, quantitative analysis of oxidized PTPs (numbers of gold particles per μm^2) in control cells or antigen (*Ag*)- or Pv-activated cells. Binding of oxPTP mAb to membrane sheets from Pv-activated cells in the presence of control (*con.*) peptide (VHCSAG) or the same peptide with Cys oxidized to sulfonic acid (*ox. peptide*) is also shown. Means ± S.D. were calculated from three independent experiments, each 22.2 mm^2. Statistical significance of intergroup differences was calculated using Student's *t* test: *, $p < 0.01$; **, $p < 0.0001$.

inhibited the binding of the oxPTP mAb to membrane sheets from pervanadate-activated cells (Fig. 9*G*), confirming the specificity of this interaction.

To determine whether oxidized PTPs are co-localized with FcεRI, the FcεRI and oxidized phosphatases were labeled on the extracellular and cytoplasmic sides, respectively, of the plasma membrane sheets isolated from pervanadate-activated cells. Under these conditions, most of FcεRI was located in distinct osmiophilic regions, whereas oxidized phosphatases were associated with membrane cytoskeleton-like structures (Fig. 9*D*). However, in a small fraction of FcεRI clusters, oxidized phosphatases were also present (Fig. 9, *E* and *F*), suggesting a functional link.

In an attempt to identify whether oxidized phosphatases are associated with actin cytoskeleton, plasma membrane sheets were labeled on the cytoplasmic side simultaneously with biotin-labeled phalloidin, which specifically reacts with F-actin (58–60), and oxPTP mAb. Data presented in Fig. 10*A* indicate that osmiophilic cytoskeleton-like structures possess both oxidized PTPs and F-actin. These data suggest that oxidized phosphatases associate with actin cytoskeleton.

One of the phosphatases detectable on isolated plasma membrane sheets is SHP-2 (Fig. 10*B*). This phosphatase was, however, localized outside osmiophilic cytoskeleton-like structures carrying oxidized phosphatases. In nonactivated as well as activated cells, SHP-2 was found mostly in areas different from those containing FcεRI (data not shown). Interestingly, a clear co-localization was occasionally observed (Fig. 10, *C* and *D*). Quantitative analysis revealed that in the course of pervanadate-mediated activation, the number of gold particles associated with SHP-2 significantly increased (Fig. 10*E*). This increase reflected specific binding of anti-SHP-2 antibody to the target antigen, because the binding was significantly reduced by addition of the corresponding blocking peptide (sc-280 P) but not negative control peptide (sc-287 P). An increased binding of oxPTP mAb to membrane sheets was also observed in antigen-activated cells; however, due to variations, this increase was insignificant.

DISCUSSION

The binding of a multivalent antigen to IgE-FcεRI complexes induces tyrosine phosphorylation of the receptor subunits. However, it is not exactly clear how the binding is communicated across the plasma membrane to the cellular interior as the

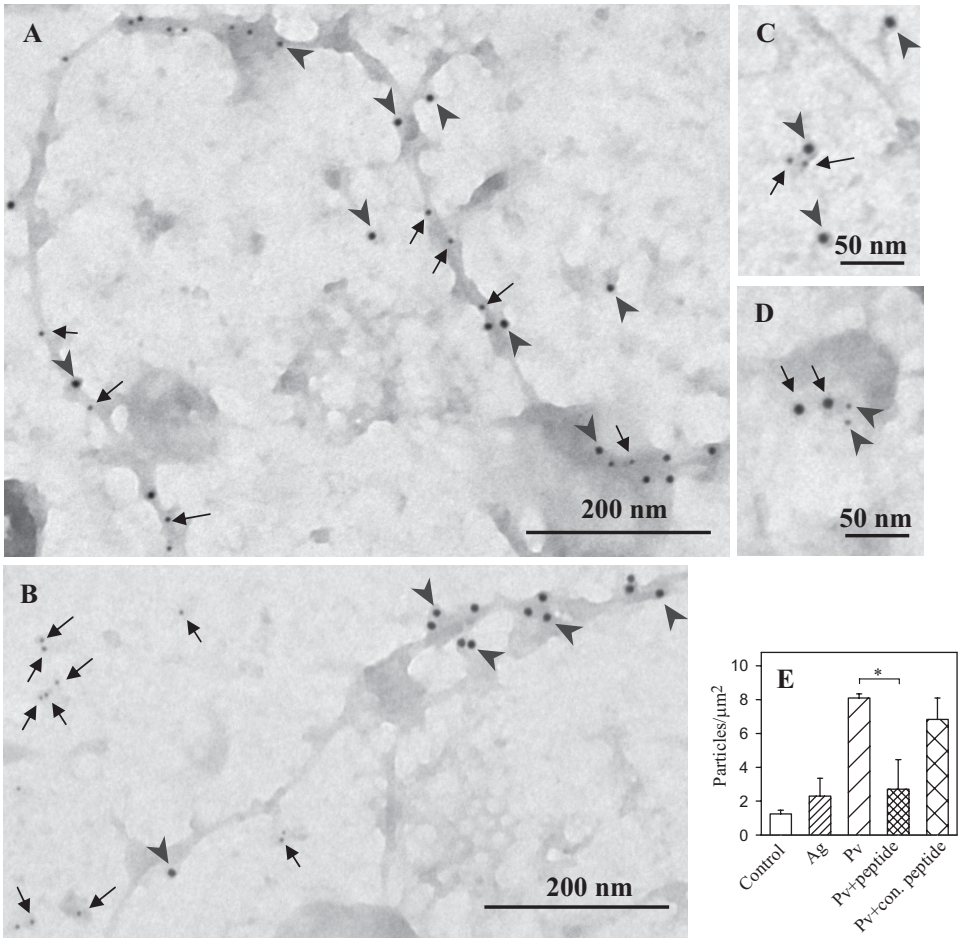

FIGURE 10. **Association of PTPs with actin cytoskeleton and FcεRI.** *A*, plasma membrane sheets were isolated from pervanadate-activated (0.2 mM, 5 min) BMMCs. The sheets were labeled from the cytoplasmic side for oxidized PTPs with oxPTP mAb followed by GαMIgG conjugated with 12-nm gold particles (*arrowheads*) and for F-actin with biotin-labeled phalloidin, followed by streptavidin conjugated with 5-nm gold particles (*arrows*). *B*, BMMCs were activated with pervanadate (as in *A*), and plasma membrane sheets were labeled with oxPTP mAb (12 nm gold, *arrowheads*) and rabbit anti-SHP-2 Ab (6 nm gold, *arrows*). *C*, plasma membrane sheets were isolated from resting cells and stained on cytoplasmic side with mouse anti-FcεRI-β mAb followed by GαMIgG conjugated with 12-nm gold particles (*arrowheads*), and rabbit anti-SHP-2 Ab followed by GαRIgG conjugated with 6-nm gold particles (*arrows*). *D*, alternatively, plasma membrane sheets were isolated from resting cells and stained on cytoplasmic side with mouse anti-FcεRI-β mAb (6 nm gold; *arrowheads*) and rabbit anti-SHP-2 Ab (12 nm gold; *arrows*). *Scale bars* are shown at the *bottom*. *E*, quantitative analysis of SHP-2 (numbers of gold particles per μm^2) in control cells or antigen (Ag)- or Pv-activated cells. Binding of SHP-2 antibody to the membrane sheets from Pv-activated cells in the presence of SHP-2 blocking peptide (*peptide*) or negative control (*con.*) peptide is also shown. Means ± S.D. were calculated from three independent experiments; each 22.2 μm^2. Statistical significance of intergroup differences was calculated using Student's *t* test, *, $p < 0.01$.

two models, which have been proposed (see Introduction and Fig. 11, *A* and *B*), are not capable of completely explaining all current observations, including those presented in this study.

To better understand the early activation events in all their complexities, we studied the role of PTPs in mast cell triggering. The oxidative agent pervanadate is known to induce protein tyrosine phosphorylation, formation of inositol 1,4,5-trisphosphate, an increase in calcium influx, and histamine secretion (11, 61). Several lines of evidence presented in this study indicate that pervanadate and H_2O_2 initiate FcεRI tyrosine phosphorylation by a mechanism that is different from the previously postulated models of FcεRI triggering.

First, exposure of the cells to the PTP inhibitor pervanadate induced tyrosine phosphorylation of FcεRI in the absence of the receptor aggregation, as evidenced by electron microscopy on isolated plasma membrane sheets. Thus, it is unlikely that tyrosine phosphorylation of the receptor subunits in pervanadate-stimulated cells is mediated by enhanced aggregation of FcεRI and associated Lyn kinase, as proposed by the transphosphorylation model (14). It is in line with previous data showing that dimerization of FcεRI leads to tyrosine phosphorylation in the absence of extensive receptor clustering (23). Thus, formation of large aggregates of multivalent antigen-IgE-FcεRI complexes within osmiophilic regions containing other signaling molecules (phospholipase Cγ2, phosphatidylinositol 3-kinase, Gab2, and Grb2) (62) is not a necessary condition for initiation of FcεRI signaling.

Second, in unstimulated cells lysed in Triton X-100, most of FcεRI is soluble and is localized in high density fractions after sucrose density gradient ultracentrifugation. Following FcεRI aggregation (by multivalent antigen-IgE complexes, antibodies against FcεRI, or biotinylated IgE-streptavidin complexes), the major part of FcεRI is associated with low density fractions (19, 24, 63). Because the same fractions also possess Lyn kinase and other signaling molecules, including some adaptor proteins (24, 64, 65), it was postulated that coalescence of FcεRI with lipid rafts is the key step for tyrosine phosphorylation of FcεRI β and γ subunits (see lipid raft model, Fig. 11*B*). However, our data indicate that exposure of mast cells to pervanadate leads to rapid tyrosine phosphorylation of the FcεRI (Fig. 1, *D* and *E*) without enhanced association of the receptor with Lyn kinase-containing DRMs (Fig. 1, *F* and *G*).

Third, the transphosphorylation model postulates that a fraction of Lyn is preassociated with FcεRI in quiescent cells (14). However, when detergent-solubilized nonactivated cells are fractionated by density gradient centrifugation, most of Lyn is found associated with DRMs in low density fractions, whereas FcεRI is found mostly in separate high density fractions (Fig. 1*F*). The latter data are in conflict with the results of electron microscopy studies indicating preassociation of a fraction of Lyn with FcεRI clusters (17), as well as with immunochemical studies detecting Lyn in immunocomplexes of FcεRI in quiescent cells (14, 16). These discrepancies can be explained by removal of Lyn from FcεRI complexes during density gradi-

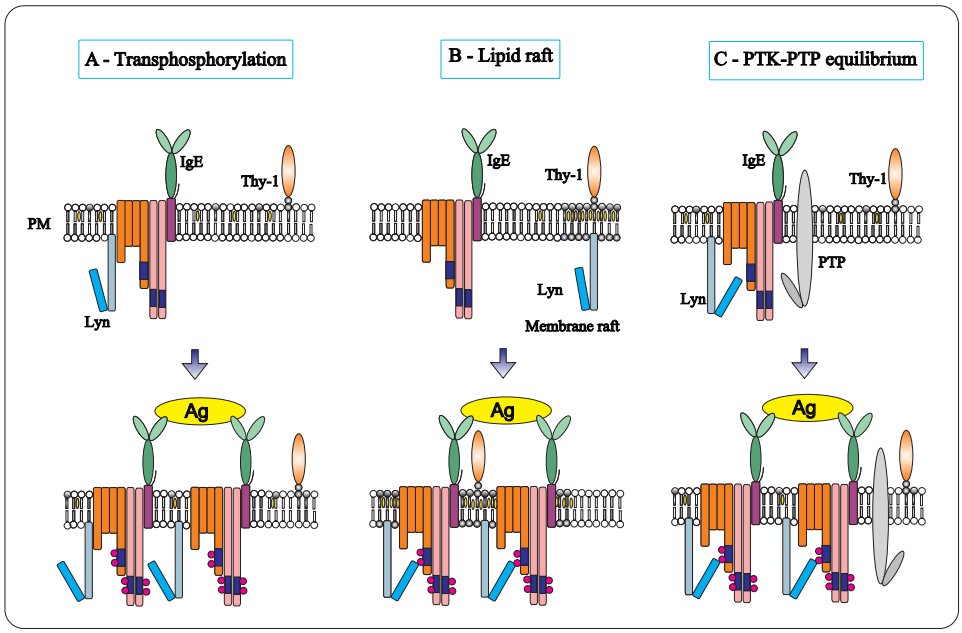

FIGURE 11. **Models of the initial tyrosine phosphorylation of the FcεRI.** *A*, according to the "transphosphorylation model," a fraction of the tetrameric FcεRI ($\alpha\beta2\gamma$) in the plasma membrane (*PM*) is associated with Lyn kinase. After binding of the IgE to the FcεRI α subunit, the receptor remains randomly distributed at the plasma membrane. Stimulation with bivalent or multivalent antigen (*Ag*) leads to receptor dimerization or multimerization. Only in the clusters can the Lyn kinases phosphorylate ITAMs of the neighboring receptors. Monovalent ligands do not cluster the receptors and therefore do not induce phosphorylation and activation. *B*, "lipid raft model" proposes that Lyn kinase is not bound to FcεRI but is separated instead into membrane regions (lipid rafts), which are enriched with cholesterol and glycosphingolipids. These domains possess some other lipid-anchored molecules, like glycosylphosphatidylinositol-anchored Thy-1 glycoprotein. After antigen-mediated FcεRI clustering, the receptors are recruited into lipid rafts where their ITAMs are phosphorylated by Lyn. *C*, according to "PTK-PTP equilibrium model," a fraction of Lyn kinase in resting cells is associated with FcεRI and phosphorylates it. This activity is counterbalanced by the action of PTPs, resulting in the formation of a basal equilibrium in quiescent cells. Perturbation of this equilibrium by inhibiting the enzymatic activity of the PTPs or by clustering-induced allosteric changes in the receptor shifts the balance between phosphorylation and dephosphorylation resulting in a net increase in tyrosine phosphorylation of the receptor.

ent fractionation of detergent-solubilized cells. Our results showing that various detergents have different effects on the binding of several tyrosine-phosphorylated proteins to the FcεRI immunocomplexes (Fig. 1*A*) support this explanation. The combined data indicate that transphosphorylation and the lipid raft model do not fully comply with all data on the mechanism of FcεRI tyrosine phosphorylation gathered under some particular conditions and that phosphatases obviously play a key role at initial stage of the activation process.

Based on these data we propose a third model for FcεRI triggering (Fig. 11*C*). According to this PTK-PTP equilibrium model, FcεRI in quiescent cells is functionally associated with PTKs and PTPs that are in equilibrium, and therefore, no net phosphorylation of FcεRI is observed. When the cell is activated, this equilibrium is disturbed, and a shift occurs in favor of kinases; consequently, FcεRI becomes phosphorylated. The first step of the activation sequence according to this model is inhibition of enzymatic activity of PTPs. ROS produced by macrophages in the close vicinity of mast cells could represent potent inhibitors of PTPs (25). ROS are also produced in the course of FcεRI triggering by mast cells, but because they are not necessary for cell triggering (66), the role of intracellular ROS production in cell activation is unclear. An alternative possibility is that activation induces conformational changes in the receptor subunits (67), either impairing (PTPs) or enhancing (PTKs) access of the enzymes to the ITAMs of the receptor, leading thus to a change in equilibrium between PTKs and PTPs and to enhanced tyrosine phosphorylation. It should be mentioned that the regulatory role of PTPs and ROS has been proposed during activation in other MIRRs (45, 68). However, our data prove for the first time that FcεRI in ROS-treated cells does not aggregate and that extensive phosphorylation of the receptor does not require its associate with Lyn-containing DRMs.

An analysis of binding motifs in nonphosphorylated FcεRI β and γ chains did not reveal any binding sites for phosphatases besides the phosphotyrosine motifs. Furthermore, we failed in attempts to co-immunoprecipitate PTPs associated with FcεRI from nonactivated cells.[5] This could reflect weak association and sensitivity to detergents used for cell solubilization. Similarly, Syk kinase, for example, which clearly interacts with FcεRI γ chain, does not co-precipitate with the receptor (56). The vicinity of FcεRI phosphotyrosine motifs may be sufficient to stimulate substrate-specific binding of PTPs. Barr *et al.* (69) provided convincing evidence that, despite the largely conserved fold, surface properties of PTP phosphatase domains are strikingly diverse. The activity of individual PTP catalytic domains against various phosphopeptides, including substrates commonly found in mast cells, such as c-Kit, WASP, or Csk, varied at least by 2 orders of magnitude. Interestingly, the reaction rates did not correlate with the specific activity of each PTP domain toward general PTP substrate 6,8-difluoro-4-methylumbelliferyl phosphate. Thus, it is possible that the PTPs in the vicinity of FcεRI recognize specific phosphorylation sites in the absence of another binding motif.

Using mAb specific for the oxidized active site cysteine of PTPs, we found a dramatic increase of oxidized phosphatases in pervanadate-treated cells. PTPs were also oxidized in both H_2O_2- and antigen-activated cells, although to lesser extent. Interestingly, most of oxidized PTPs were found in the high density fractions of sucrose gradients, suggesting that they are separated from signaling assemblies during cell solubilization and/or density gradient fractionation. It is possible that oxidation of the PTPs modifies their physical properties and contributes to their relocation to actin cytoskeleton (see below) and cytoplasm.

[5] P. Heneberg, L. Dráberová, and P. Dráber, unpublished data.

DRMs are known to host only a fraction of total membrane and submembrane PTPs. Peirce and Metzger (56) suggested that tyrosine phosphorylation of substrates located in DRMs is favored by both the enrichment of kinases and the paucity of phosphatases; however, several pieces of evidence do not support such model. Only a limited fraction of PTPs (see *e.g. SHP-1* in Fig. 5) is associated with DRMs. Furthermore, membrane proteins located outside DRMs are dephosphorylated with the similar kinetics as phosphoproteins residing in DRMs (56). Finally, the DRM-associated pool of PTPs is largely in reduced form (Fig. 5), allowing its higher enzymatic activity and faster fine-tuning by phosphorylation and/or conformational changes. Therefore, it is possible that plasma membrane hosts a fraction of PTPs, which undergo strict regulation of their activity in activated cells. Alternatively, oxidation leads to the removal of PTPs from DRMs, contributing to the observed deficiency of oxidized PTPs in DRMs (56, 70).

Does FcεRI triggering resemble signaling via the growth factor receptors (7, 53, 53, 71) and does it also lead to inactivation of PTPs via ROS species? Our results, as well as data from others (25, 66, 72), clearly show that there is an increase in the amount of oxidized PTPs in antigen-activated mast cells. However, the results presented here also indicate that despite the fact that a fraction of phosphatases is oxidized and thus inactivated, the net enzymatic activity is not necessarily reduced and is largely dependent on other ways of regulation, leading to either an increase (SHP-2) or a decrease (HePTP) in their enzymatic activity after FcεRI triggering. It is therefore likely that under physiological conditions only a limited fraction of PTPs is inactivated by oxidation. This corresponds with the findings that physiological concentrations of ROS are not capable of inducing oxidation of the whole pool of particular PTPs (73). Thus, in the course of MIRRs or growth factor receptor activation, cells may retain a pool of PTPs with reduced active site cysteines that undergo versatile regulation based on conformational and/or phosphorylation changes leading to a further increase or decrease of their enzymatic activity by several orders of magnitude (74).

The unexpected finding reported here is the association of PTPs recognized by oxPTP mAb predominantly with plasma membrane actin cytoskeleton. Although detailed identification of the target phosphatases will require further studies, it is possible that actin cytoskeleton is involved in early activation events by regulating the topography of phosphatases. Interestingly, FcεRI was only rarely co-localized with PTPs or their oxidized forms. However, such co-localization was occasionally observed (Fig. 9, *E* and *F*, and Fig. 10, *C* and *D*), confirming a physical and functional link between PTPs and FcεRI.

In summary, we propose an alternative pathway of an initial stage of FcεRI triggering based on the existence of preformed complexes containing FcεRI, PTKs, and PTPs, where the latter two components are in equilibrium in quiescent cells. Activation-induced down-regulation of the enzymatic activity of PTPs by oxidation of their active site cysteine and/or changes in their accessibility to the receptor subunits lead to disturbance of the equilibrium and subsequently enhanced tyrosine phosphorylation of the receptor subunits.

Acknowledgments—We thank Hana Mrázová and Romana Budovičová for expert technical assistance.

REFERENCES

1. Gilfillan, A. M., and Tkaczyk, C. (2006) *Nat. Rev. Immunol.* **6,** 218–230
2. Gilfillan, A. M., and Rivera, J. (2009) *Immunol. Rev.* **228,** 149–169
3. Heneberg, P., and Dráber, P. (2002) *Int. Arch. Allergy Immunol.* **128,** 253–263
4. Pao, L. I., Badour, K., Siminovitch, K. A., and Neel, B. G. (2007) *Annu. Rev. Immunol.* **25,** 473–523
5. Vang, T., Miletic, A. V., Arimura, Y., Tautz, L., Rickert, R. C., and Mustelin, T. (2008) *Annu. Rev. Immunol.* **26,** 29–55
6. Denu, J. M., and Tanner, K. G. (1998) *Biochemistry* **37,** 5633–5642
7. Meng, T. C., Fukada, T., and Tonks, N. K. (2002) *Mol. Cell* **9,** 387–399
8. Zick, Y., and Sagi-Eisenberg, R. (1990) *Biochemistry* **29,** 10240–10245
9. Heffetz, D., Bushkin, I., Dror, R., and Zick, Y. (1990) *J. Biol. Chem.* **265,** 2896–2902
10. Teshima, R., Ikebuchi, H., Nakanishi, M., and Sawada, J. (1994) *Biochem. J.* **302,** 867–874
11. Amoui, M., Dráberová, L., Tolar, P., and Dráber, P. (1997) *Eur. J. Immunol.* **27,** 321–328
12. Huyer, G., Liu, S., Kelly, J., Moffat, J., Payette, P., Kennedy, B., Tsaprailis, G., Gresser, M. J., and Ramachandran, C. (1997) *J. Biol. Chem.* **272,** 843–851
13. Eiseman, E., and Bolen, J. B. (1992) *Nature* **355,** 78–80
14. Pribluda, V. S., Pribluda, C., and Metzger, H. (1994) *Proc. Natl. Acad. Sci. U.S.A.* **91,** 11246–11250
15. Sil, D., Lee, J. B., Luo, D., Holowka, D., and Baird, B. (2007) *ACS Chem. Biol.* **2,** 674–684
16. Vonakis, B. M., Gibbons, S. P., Jr., Rotté, M. J., Brothers, E. A., Kim, S. C., Chichester, K., and MacDonald, S. M. (2005) *J. Immunol.* **175,** 4543–4554
17. Wilson, B. S., Pfeiffer, J. R., and Oliver, J. M. (2000) *J. Cell Biol.* **149,** 1131–1142
18. Field, K. A., Holowka, D., and Baird, B. (1995) *Proc. Natl. Acad. Sci. U.S.A.* **92,** 9201–9205
19. Field, K. A., Holowka, D., and Baird, B. (1997) *J. Biol. Chem.* **272,** 4276–4280
20. Simons, K., and Toomre, D. (2000) *Nat. Rev. Mol. Cell Biol.* **1,** 31–39
21. Munro, S. (2003) *Cell* **115,** 377–388
22. Brown, D. A. (2006) *Physiology* **21,** 430–439
23. Dráberová, L., Lebduška, P., Hálová, I., Tolar, P., Štokrová, J., Tolarová, H., Korb, J., and Dráber, P. (2004) *Eur. J. Immunol.* **34,** 2209–2219
24. Kovářová, M., Tolar, P., Arudchandran, R., Dráberová, L., Rivera, J., and Dráber, P. (2001) *Mol. Cell. Biol.* **21,** 8318–8328
25. Swindle, E. J., Hunt, J. A., and Coleman, J. W. (2002) *J. Immunol.* **169,** 5866–5873
26. Swieter, M., Berenstein, E. H., Swaim, W. D., and Siraganian, R. P. (1995) *J. Biol. Chem.* **270,** 21902–21906
27. Xie, Z. H., Zhang, J., and Siraganian, R. P. (2000) *J. Immunol.* **164,** 1521–1528
28. Kimura, T., Zhang, J., Sagawa, K., Sakaguchi, K., Appella, E., and Siraganian, R. P. (1997) *J. Immunol.* **159,** 4426–4434
29. Nakata, K., Yoshimaru, T., Suzuki, Y., Inoue, T., Ra, C., Yakura, H., and Mizuno, K. (2008) *J. Immunol.* **181,** 5414–5424
30. Barsumian, E. L., Isersky, C., Petrino, M. G., and Siraganian, R. P. (1981) *Eur. J. Immunol.* **11,** 317–323
31. Chen, T. R. (1977) *Exp. Cell Res.* **104,** 255–262
32. Rudolph, A. K., Burrows, P. D., and Wabl, M. R. (1981) *Eur. J. Immunol.* **11,** 527–529
33. Liu, F. T., Bohn, J. W., Ferry, E. L., Yamamoto, H., Molinaro, C. A., Sherman, L. A., Klinman, N. R., and Katz, D. H. (1980) *J. Immunol.* **124,** 2728–2737
34. Dráberová, L., Amoui, M., and Dráber, P. (1996) *Immunology* **87,** 141–148
35. Rivera, J., Kinet, J. P., Kim, J., Pucillo, C., and Metzger, H. (1988) *Mol. Immunol.* **25,** 647–661
36. Andersen, J. N., Mortensen, O. H., Peters, G. H., Drake, P. G., Iversen, L. F.,

Olsen, O. H., Jansen, P. G., Andersen, H. S., Tonks, N. K., and Møller, N. P. (2001) *Mol. Cell. Biol.* **21,** 7117–7136
37. Persson, C., Kappert, K., Engström, U., Östman, A., and Sjöblom, T. (2005) *Methods* **35,** 37–43
38. Lebduška, P., Korb, J., Tůmová, M., Heneberg, P., and Dráber, P. (2007) *J. Immunol. Methods* **328,** 139–151
39. Philimonenko, A. A., Janáček, J., and Hozák, P. (2000) *J. Struct. Biol.* **132,** 201–210
40. Dráberová, L., Dudková, L., Boubelík, M., Tolarová, H., Šmíd, F., and Dráber, P. (2003) *J. Immunol.* **171,** 3585–3593
41. Weibrecht, I., Böhmer, S. A., Dagnell, M., Kappert, K., Östman, A., and Böhmer, F. D. (2007) *Free Radic. Biol. Med.* **43,** 100–110
42. Tolarová, H., Dráberová, L., Heneberg, P., and Dráber, P. (2004) *Eur. J. Immunol.* **34,** 1627–1636
43. Suzuki, Y., Yoshimaru, T., Matsui, T., Inoue, T., Niide, O., Nunomura, S., and Ra, C. (2003) *J. Immunol.* **171,** 6119–6127
44. O'Shea, J. J., McVicar, D. W., Bailey, T. L., Burns, C., and Smyth, M. J. (1992) *Proc. Natl. Acad. Sci. U.S.A.* **89,** 10306–10310
45. Wienands, J., Larbolette, O., and Reth, M. (1996) *Proc. Natl. Acad. Sci. U.S.A.* **93,** 7865–7870
46. Dráber, P., Dráberová, L., Heneberg, P., Šmíd, F., Farghali, H., and Dráber, P. (2007) *Cell. Signal.* **19,** 2400–2412
47. Antunes, F., and Cadenas, E. (2000) *FEBS Lett.* **475,** 121–126
48. Wilson, B. S., Pfeiffer, J. R., Surviladze, Z., Gaudet, E. A., and Oliver, J. M. (2001) *J. Cell Biol.* **154,** 645–658
49. Surviladze, Z., Harrison, K. A., Murphy, R. C., and Wilson, B. S. (2007) *J. Lipid Res.* **48,** 1325–1335
50. Mikalsen, S. O., and Kaalhus, O. (1998) *J. Biol. Chem.* **273,** 10036–10045
51. Heneberg, P., and Dráber, P. (2005) *Curr. Med. Chem.* **12,** 1859–1871
52. Tonks, N. K. (2005) *Cell* **121,** 667–670
53. Persson, C., Sjöblom, T., Groen, A., Kappert, K., Engström, U., Hellman, U., Heldin, C. H., den Hertog, J., and Östman, A. (2004) *Proc. Natl. Acad. Sci. U.S.A.* **101,** 1886–1891
54. Keilhack, H., Müller, M., Böhmer, S. A., Frank, C., Weidner, K. M., Birchmeier, W., Ligensa, T., Berndt, A., Kosmehl, H., Günther, B., Müller, T., Birchmeier, C., and Böhmer, F. D. (2001) *J. Cell Biol.* **152,** 325–334
55. Simoneau, M., Boulanger, J., Coulombe, G., Renaud, M. A., Duchesne, C., and Rivard, N. (2008) *J. Biol. Chem.* **283,** 25544–25556
56. Peirce, M., and Metzger, H. (2000) *J. Biol. Chem.* **275,** 34976–34982
57. Gulati, P., Markova, B., Göttlicher, M., Böhmer, F. D., and Herrlich, P. A. (2004) *EMBO Rep.* **5,** 812–817
58. Wulf, E., Deboben, A., Bautz, F. A., Faulstich, H., and Wieland, T. (1979) *Proc. Natl. Acad. Sci. U.S.A.* **76,** 4498–4502
59. Lachapelle, M., and Aldrich, H. C. (1988) *J. Histochem. Cytochem.* **36,** 1197–1202
60. Steinmetz, M. O., Stoffler, D., Müller, S. A., Jahn, W., Wolpensinger, B., Goldie, K. N., Engel, A., Faulstich, H., and Aebi, U. (1998) *J. Mol. Biol.* **276,** 1–6
61. den Hertog, J., Groen, A., and van der Wijk, T. (2005) *Arch. Biochem. Biophys.* **434,** 11–15
62. Wilson, B. S., Pfeiffer, J. R., and Oliver, J. M. (2002) *Mol. Immunol.* **38,** 1259–1268
63. Field, K. A., Holowka, D., and Baird, B. (1999) *J. Biol. Chem.* **274,** 1753–1758
64. Volná, P., Lebduška, P., Dráberová, L., Šímová, S., Heneberg, P., Boubelík, M., Bugajev, V., Malissen, B., Wilson, B. S., Hořejší, V., Malissen, M., and Dráber, P. (2004) *J. Exp. Med.* **200,** 1001–1013
65. Zhang, W., Sloan-Lancaster, J., Kitchen, J., Trible, R. P., and Samelson, L. E. (1998) *Cell* **92,** 83–92
66. Swindle, E. J., Coleman, J. W., DeLeo, F. R., and Metcalfe, D. D. (2007) *J. Immunol.* **179,** 7059–7071
67. Tolar, P., Sohn, H. W., and Pierce, S. K. (2005) *Nat. Immunol.* **6,** 1168–1176
68. Reth, M. (2002) *Nat. Immunol.* **3,** 1129–1134
69. Barr, A. J., Ugochukwu, E., Lee, W. H., King, O. N., Filippakopoulos, P., Alfano, I., Savitsky, P., Burgess-Brown, N. A., Müller, S., and Knapp, S. (2009) *Cell* **136,** 352–363
70. Stauffer, T. P., and Meyer, T. (1997) *J. Cell Biol.* **139,** 1447–1454
71. Chen, C. H., Cheng, T. H., Lin, H., Shih, N. L., Chen, Y. L., Chen, Y. S., Cheng, C. F., Lian, W. S., Meng, T. C., Chiu, W. T., and Chen, J. J. (2006) *Mol. Pharmacol.* **69,** 1347–1355
72. Swindle, E. J., Metcalfe, D. D., and Coleman, J. W. (2004) *J. Biol. Chem.* **279,** 48751–48759
73. Lou, Y. W., Chen, Y. Y., Hsu, S. F., Chen, R. K., Lee, C. L., Khoo, K. H., Tonks, N. K., and Meng, T. C. (2008) *FEBS J.* **275,** 69–88
74. Barford, D., and Neel, B. G. (1998) *Structure* **6,** 249–254